Computational Particle Mechanics (2024) 11:1–27
https://doi.org/10.1007/s40571-023-00606-w

An investigation of compliant contact force models applied for analysis of simultaneous, multi-zone impacts of particles

Mariusz Warzecha[1]

Received: 29 November 2022 / Revised: 26 April 2023 / Accepted: 27 April 2023 / Published online: 6 June 2023

Abstract
Compliant contact force models were developed and mainly used to investigate simple impacts of two bodies. It is therefore unclear how they will perform in more complex cases, where simultaneous, multi-zone impact may occur. The aim of this study is to investigate phenomena that occur in such impacts and to study the effectiveness of preselected contact force models in their modelling. For this purpose, the study addressed collisions that occur in a collinear system of 3 to 6 particles made of steel, aluminium, and bronze. The results obtained for each force model were referenced to the FEM analysis. To compare the performance of the models, the Benchmark Velocity Indicator (BVI) is proposed. The study showed that during simultaneous, multi-zone impact direct switch from the restitution to compression phases may occur and subsequent collision along the same normal may take place. Such phenomena are not incorporated in current compliant contact force models; therefore, the study showed the need for their further improvement. The best models proposed by Kogut and Etsion (KE) and Jackson and Green (JG) achieved average errors equal to 3.89% and 4.15%, respectively. However, the same models in their worst cases reached error values of 38.66% and 33.77%. The article concludes with proposals for future improvements.

Keywords Simultaneous impact · Multi-zone collision · Contact force model · Multibody system · Particle chain

List of symbols

F_n	Normal contact force
F_{nm}	Normal contact force at the compression end time instant
F_{ny}	Normal contact force at the start of a material yield
$\delta, \dot{\delta}, \ddot{\delta}$	Relative displacement of contacting particles and its time derivatives
δ_y	Relative displacement of contacting particles where yielding occurs
δ_m	Maximum relative displacement of contacting particles (maximum deformation)
δ_r	Permanent (residual) deformation
K	Contact stiffness
χ	Damping factor
c_r	Coefficient of restitution
$\dot{\delta}_0, \dot{\delta}_f$	Initial and final particle relative velocity
S_y	Material yield strength
E^*	Effective contact modulus
R	Particle radius
R^*	Effective radius
R_r^*	Effective, deformed radius of curvature
m^*	Effective particle mass
H_G	Hardness geometric limit
H	Hardness
ν	Material Poisson ratio
ρ	Material density
a	Radius of contact area

✉ Mariusz Warzecha
mwarzech@agh.edu.pl

[1] AGH University of Science and Technology, Faculty of Mechanical Engineering and Robotics, Mickiewicza 30 Ave, 30-059 Kraków, Poland

1 Introduction

Impact is a phenomenon commonly occurring during the work of various mechanical systems. Its sources can often be rooted in clearances present in mechanical joints due to manufacturing tolerances or wear [1–3]. In some cases, impact is bound with the main function of machines, as is the case in inertial grids and hammer crushers etc. [4] or in linear particle chain impact dampers [5–7]. Impact-contact problems

are also crucial in predicting behaviour of granular media [8–17], aircraft wing behaviour after bird strikes [18], human safety [19] or wheel-rail interaction [20, 21]. Regardless of the impact source, its modelling poses a challenging problem.

There are several approaches described in the literature used for modelling impacts in a multi-body system. They can be divided into two main groups: non-smooth approaches and smooth approaches. In the former case, the coefficient of restitution (COR) is used to calculate the energy amount dissipated during the impact and determine the body velocities after its termination. In the latter case, an assumption is made that colliding bodies are compliant in the vicinity of the impact points. This allows determination of the impact duration, and evaluation of impact force in time.

The application of non-smooth approaches in a multibody system requires an additional assumption. The impacts must be considered one by one (sequentially) or all of them must take place exactly at the same time (simultaneously). Both assumptions were applied in various studies [22–25], but it has been shown that each of them gives reasonable results only when certain conditions are satisfied [26, 27].

The smooth approaches require the continuous contact force model to represent the impact force. Many such models have been proposed [28–48]. Several works applied smooth approaches for analysis of multi-zone impact. Stronge [49] used bi-linear and non-linear Hertz spring elements to represent local deformation in the model of impact in a collinear system consisting of up to six touching particles. It showed that non-smooth (momentum-based) approaches give reasonable results in such systems only when certain conditions are satisfied. Analysis of the temporal variation in velocity for each element indicated dispersion and negative residual velocity decreasing exponentially with the distance from the initiating impact. Carreto-Gonzalez et al. [50] measured the propagation of solitary waves in a chain of small particles impacted by a striker. They reported results for chains containing 70 particles made of stainless steel, Teflon, and brass. Those results were used to obtain damping parameters in a contact force model used to simulate system behaviour. The proposed model was based on a Hertz non-linear spring element augmented with a non-linear damping force. A contact force model expressing energy dissipation by plastic deformation was used in [8] for numerical simulation of 1D chains of particles. The empirical parameters of this model, described in [51], were obtained by finite element method (FEM). The simulation results were validated by measurements of system behaviour impacted by the Hopkinson bar. An elastic–plastic contact model was also used in analogous simulations by Feng et al. [52]. The authors stated in the conclusions that such a model has sufficient accuracy to model wave propagation in granular systems, however, parameters fitting the experimental data were used to obtain the model.

Although contact force models have been used for simulating multi-zone impacts, it is not clear if they are suitable for this purpose, because they were usually validated by comparison of experimental data obtained from the impact of two bodies (usually particles) with numerical results calculated by their implementation in simulations. Because the impact event is highly non-linear, it can be expected that superposition will have limited applicability. Therefore, comprehensive analysis is needed to systematically study the behaviour of the available models in multi-zone impacts. As such a study is currently non-existent, this article aims to fill that gap.

The present work compares the available contact force models in application to multi-zone impact. The goal of the work is to outline the models that are most suitable in the description of such events and identify phenomena influencing their accuracy. Moreover, the article proposes methodology that can be used in future validation of the new and improved contact force models. The analysis focuses on compact bodies and impact velocities significantly smaller than the velocity of elastic waves propagating through the impacting bodies, as the validity of analysed models was investigated for such cases in two-body impacts. The investigated system consisted of up to 6 particles (beads).

This study is organized as follows: in the next section the selection process of the contact force models is described, all the selected contact force models are outlined, and their parameters are examined, Sect. 3 introduces FEM analysis for two particles to check how well the results obtained by numerical simulation implementing the analysed model and FEM analysis results correlate to each other. Section 4 compares the results obtained from the simulation of impact in 1D particle chains consisting of up to 6 particles for various contact force models with those obtained by FEM analysis. Section 5 discusses the obtained results and is followed by Conclusions.

2 Selection of contact force models for analysis

A contact force model plays an important role in the numerical simulation of impact. Its importance has been acknowledged by many works proposing improved constitutive relations [43]. Most of them are based on Hertz contact law, which is commonly agreed to correctly model purely elastic cases. As such cases are rare in practical systems, a contact force model must be augmented by a term allowing energy dissipation. There have been two main approaches to achieve this goal: inclusion of a damping force or plastic deformation. Both have been used in numerous contact force models.

The contact force model proposed by Hunt and Crosley [29] became a ground for the development of models expressing energy dissipation using a damping force. The constitutive law of this model was given in Eq. (1). To ensure that contact force is equal 0 at the beginning of impact, the relative velocity of impacting bodies was multiplied by nonlinear relative displacement. The damping factor χ was given by Eq. (2). It expressed the amount of dissipated energy by the coefficient of restitution (COR) and its refinement turned out to be the main model development area. Other relations expressing the damping factor χ were proposed by: Herbert and McWhannell [53], Lee and Wang [54], Lankarani and Nikravesh [55], Gonthier [56], Zhiying and Qishao [57], Flores et al. [30], Hu and Guo [31], Shen et al. [58], Carvalho and Martins [32], Safaeifar and Farshidianfar [59] and Zhang et al. [60].

$$F_n = K\delta^{\frac{3}{2}} + \chi\delta^{\frac{3}{2}}\dot{\delta} \tag{1}$$

$$\chi = \frac{3}{2}\frac{K}{\dot{\delta}_0}(1 - c_r) \tag{2}$$

Several review papers compared contact force models expressing energy dissipation by the introduction of damping force [37, 40, 41, 44–46, 61, 62]. Most of those studies were based on the comparison of results obtained for various models in the impact of two bodies (usually particles) for a range of initial impact velocities and COR. Based on those reviews, the models proposed by Gonthier et al. [56], Zhiying and Qishao [57] and Flores et al. [30] were selected for further analysis. During this analysis, it was noted that all the mentioned models, except the model proposed by Jankowski, use the initial impact velocity $\dot{\delta}_0$ to determine the damping factor χ. Whereas such velocity is known a priori in two-body impact, in multi-zone impact between many bodies it is the case only for the initiating impact. For the other impacts, it cannot be stated a priori and is often equal 0 for contacting bodies. Therefore, the mentioned models are not suitable for use in modelling multi-zone impact in multi-body systems. The model proposed by Jankowski [42] requires iterative calculations for determination of the damping factor. Such a procedure is possible only for the initiating collision; therefore, this model was also excluded from analysis. A further literature review identified 3 additional contact force models proposed by: Michalczyk [63], Carvalo and Martins [32], and Zhang [60]. The first introduces energy dissipation in a different manner. It modifies the value of the Hertz stiffness coefficient between the compression and restitution phases. The models put forward by Carvalo and Zhang require the initial impact velocity $\dot{\delta}_0$ to determine the damping factor χ, although the model proposed by Zhang can be used in an approximated form without knowledge of this velocity.

Contact force models expressing energy dissipation by material plastic deformation usually divide the process into loading and unloading phases. The loading phase can be additionally subdivided into elastic, elastic–plastic, and plastic. Mathematical relations for each of those phases are usually based on results obtained from quasistatic FEM analysis verified by experimental tests [33–35, 64–69], although models based on analytical reasoning are also present in the literature [70, 71]. The investigated system is typically built from a flat part and a sphere. The materials for each of those elements are normally chosen in such a manner, that the contact can be assigned to one of two cases: indentation or flattening [72]. The contact case is called indentation if the material used for the sphere is much stiffer than the material used for the flat part. The flattening is related to the opposite situation, namely when the material used for the flat part is much stiffer than the material used for the sphere. The contact models based on flattening and indentation cases can significantly differ in the obtained results [73], especially as it is common to assume that the stiffer element is rigid [69]. Recently, Wang et al. [74] compared eighteen elastic–plastic contact models in modelling the impact of a spherical particle on a half-space. The outcomes were compared with results obtained from FEM analysis. Based on this comparison, models giving the smallest errors for maximum impact force, impact duration, maximum indentation, and coefficient of restitution (COR) were obtained. At this point, it must be stated that only one of the models predicted COR with an error smaller than 5% and there were no common models between flattening and indentation in this case. Additionally, the study showed that for the conducted simulation there was little difference between the indentation and flattening cases. The best models identified by Wang et al. for two-body impact were taken for analysis in this paper. It seems reasonable to assume that if a contact model shows a high level of error in the two-body (single zone) impact, it will show errors at least as big for more complex multi-zone impact.

3 Behaviour of selected contact force models in two-body impact

The preselection of contact models conducted in the previous section resulted in 6 models, listed in Table 1. Two of those models, MK and ZG, use COR for the expression of energy dissipation. The values of COR were obtained from FEM analysis of two impacting particles. It was shown in [75] that such an approach allows good prediction of COR, although it requires the strain rate dependent material constitutive law. Because the DW, JG, KE, and GA models were based on an ideally plastic, strain rate independent material constitutive law, it was decided to also use the same law in the FEM analysis. Focus on errors resulting from multi-zone impact

Table 1 Contact force models selected for modelling multi-zone impact. Selection based on the literature review

[DW] Du and Wang [66]	Loading phase: $F_n = \frac{4}{3}E^*(R^*)^{\frac{1}{2}}\delta^{\frac{3}{2}} for \delta < \delta_y;\ F_n = \pi R^* p_p \delta - \frac{p_p^3 \pi^3 (R^*)^2}{12(E^*)^2} for \delta_y < \delta \leq \delta_m$ Unloading phase: $F_n = \frac{4}{3}E^*(R^*)^{\frac{1}{2}}\delta^{\frac{3}{2}} if \delta_m \leq \delta_y;\ F_n = \frac{4}{3}E^*(R^*)^{\frac{1}{2}}(\delta - \delta_r)^{\frac{3}{2}} if \delta_m > \delta_y$ Parameters: $\delta_y = \left(\frac{\pi p_p}{2E^*}\right)^2 R^*;\ p_p = \left(1 + \frac{\pi}{2}\right)S_y;$ $\delta_r = \delta_m - \left[\frac{3}{4E^*(R^*)^{\frac{1}{2}}}\left(\pi R^* p_p \delta_m - \frac{p_p^3 \pi^3 (R^*)^2}{12(E^*)^2}\right)\right]^{\frac{2}{3}}$ $\delta_m = \sqrt{\left[\frac{p_p^2 \pi^2 R^*}{6(E^*)^2}\right]^2 + \frac{m^* \dot{\delta}_y^2}{p_p \pi R^*}} + \frac{p_p^2 \pi^2 R^*}{12(E^*)^2};\ \dot{\delta}_y = \sqrt{\dot{\delta}_0^2 - \frac{16E^*(R^*)^{\frac{1}{2}}}{15m^*}\delta_y^{\frac{5}{2}}}$
[GA] Ghaednia et al. [68]	Loading phase: $F_n = \frac{4}{3}E^*(R^*)^{\frac{1}{2}}\delta^{\frac{3}{2}} for \delta^* < 1.9$ $F_n = F_{ny}\left[e^{-0.17\delta^{*\frac{5}{12}}}\delta^{*\frac{3}{2}} + \frac{4H_G}{CS_y}\left(1 - e^{-\frac{1}{78}\delta^{*\frac{5}{9}}}\right)\delta^{*1.1}\right] for \delta^* \geq 1.9$ Unloading phase: $F_n = \frac{4}{3}E^*\left(R_r^*\right)^{\frac{1}{2}}(\delta - \delta_r)^{\frac{3}{2}}$ Parameters: $\delta^* = \frac{\delta}{\delta_y};\ \delta_y = \left(\frac{\pi C S_y}{2E^*}\right)^2 R^*;\ C = 1.295e^{0.736\nu};$ $\frac{H_G}{S_y} = 2.84 - 0.92\left[1 - cos\left(\pi \frac{a}{R^*}\right)\right]$ $a = \sqrt{R^*\delta(\delta^*/1.9)^B};\ B = 0.14e^{23e_y};\ e_y = \frac{S_y}{E^*};\ R_r^* = \frac{1}{(\delta_m - \delta_r)^3}\left(\frac{3F_{nm}}{4E^*}\right)^2$ $\frac{\delta_r}{\delta_m} = 0.8\left[1 - \left(\frac{\delta_m/\delta_y + 5.5}{6.5}\right)^{-2}\right]$
[JG] Jackson and Green [35] and Jackson et al. [67]	Loading phase: $F_n = \frac{4}{3}E^*(R^*)^{\frac{1}{2}}\delta^{\frac{3}{2}} for \delta^* < 1.9$ $F_n = F_{ny}\left[e^{-0.25\delta^{*\frac{5}{12}}}\delta^{*\frac{3}{2}} + \frac{4H_G}{CS_y}\left(1 - e^{-\frac{1}{25}\delta^{*\frac{5}{9}}}\right)\delta^*\right] for \delta^* \geq 1.9$ Unloading phase: $F_n = \frac{4}{3}E^*\left(R_r^*\right)^{\frac{1}{2}}(\delta - \delta_r)^{\frac{3}{2}}$ Parameters: $\delta^* = \frac{\delta}{\delta_y};\ \delta_y = \left(\frac{\pi C S_y}{2E^*}\right)^2 R^*;\ C = 1.295e^{0.736\nu};$ $\frac{H_G}{S_y} = 2.84\left[1 - e^{-0.82(a/R^*)^{-0.7}}\right]$ $\frac{a}{R^*} = \frac{\pi C e_y}{2}\sqrt{\delta^*\left(\frac{\delta^*}{1.9}\right)^B};\ B = 0.14e^{23e_y};\ e_y = \frac{S_y}{E^*};\ R_r = \frac{1}{(\delta_m - \delta_r)^3}\left(\frac{3F_{nm}}{4E^*}\right)^2$ $\frac{\delta_r}{\delta_m} = 1.02\left[1 - \left(\frac{\delta_m/\delta_y + 5.9}{6.9}\right)^{-0.54}\right]$

Table 1 (continued)

[KE] Kogut and Etison [33] and Etsion et al. [65]	Loading phase: $F_n = F_{ny}(\delta^*)^{\frac{3}{2}} for \delta^* < 1;\ F_n = 1.03F_{ny}(\delta^*)^{1.425} for 1 \le \delta^* \le 6$ $F_n = 1.40F_{ny}(\delta^*)^{1.263} for 6 < \delta^* \le 110$ Unloading phase: $F_n = F_{nm}\left(\frac{\delta^* - \delta_r^*}{\delta_m^* - \delta_r^*}\right)^{n_p}$ Parameters: $F_{ny} = \frac{4}{3}E^*(R^*)^{\frac{1}{2}}(\delta_y)^{\frac{3}{2}};\ \delta_y = \left(\frac{2.8\pi K_v S_y}{2E^*}\right)^2 R^*;\ K_v = 0.454 + 0.41\nu$ $\delta^* = \frac{\delta}{\delta_y};\ \delta_r^* = \delta_m^*\left(1 - \frac{1}{\left(\frac{\delta_m}{\delta_y}\right)^{0.28}}\right)\left(1 - \frac{1}{\left(\frac{\delta_m}{\delta_y}\right)^{0.69}}\right);\ n_p = 1.5(\delta_m^*)^{-0.0331}$
[MK] Michalczyk [63]	$F_n = K\delta^n - \chi\delta^n$ $\chi = \frac{K(1-c_r^2)}{2}(1 - sgn(\dot{\delta}))$
[ZG] Zhang et al. approximate [60]	$F_n = K\delta^n\left(\frac{1+\alpha c_r - c_r}{\alpha c_r}\right) for \dot{\delta} > 0$ $F_n = K\delta^n\left(\frac{\alpha + c_r - 1}{\alpha}\right) for \dot{\delta} \le 0$ $\alpha = 0.6181e^{-3.52c_r} + 0.899e^{0.09025c_r}$

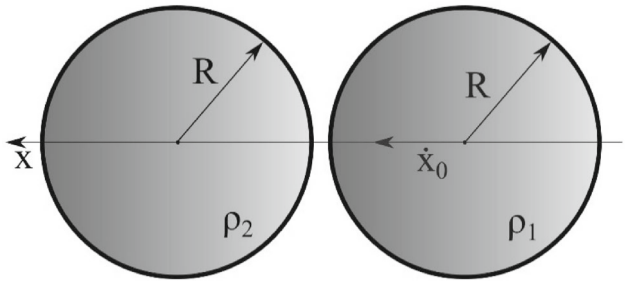

Fig. 1 The system of two impacting particles used for the determination of COR

justified such simplification as otherwise the difference in constitutive laws would manifest itself as an additional error.

This section describes the used FEM model, gives the calculated COR values, and compares impact forces resulting from FEM analysis with those obtained from implementation of contact models for the given system.

3.1 FEM model

The system used for the determination of COR consisted of two particles shown schematically in Fig. 1. Both of them had the radius R = 10 mm and were made of one of three materials: stainless steel 440C, aluminium 2014-T6 and bronze C95400. This yielded 6 different combinations, namely: steel-steel, aluminium-aluminium, bronze-bronze, aluminium-steel, steel-bronze, bronze-aluminium. The materials were chosen to achieve a wide range of contact stiffness. Their properties are given in Table 2. One of the particles was at rest, while the second impacted it with three selected velocities: 0.1 m/s, 1 m/s and 3 m/s.

Table 2 Properties of the materials selected for the particles

	Stainless steel 440C	Aluminium 2014-T6	Bronze C95400
Young modulus [GPa]	209	73.1	110
Poisson ratio [-]	0.283	0.33	0.316
Yield strength [MPa]	1175	365	205
Density [g/cm3]	7.8	2.8	7.45
Brinell hardness [kgf/mm2]	290	135	170

The particle mesh was generated in Gmsh [76]. As the simulated system was axisymmetric, the particle was modelled as half of a circle. The generated mesh, shown in Fig. 2, consisted of 18,193 quadrilateral and 856 triangular, second-order elements. The element size varied and depended on the distance from the initial contact points A and B. The smallest elements were generated in the vicinity of the initial contact points. The initial size of those elements was determined based on the smallest contact area radius at yield. The following equations were used for this purpose:

$$\delta_y = \left(\frac{\beta C S_y}{2E^*}\right)^2 R^* \tag{3}$$

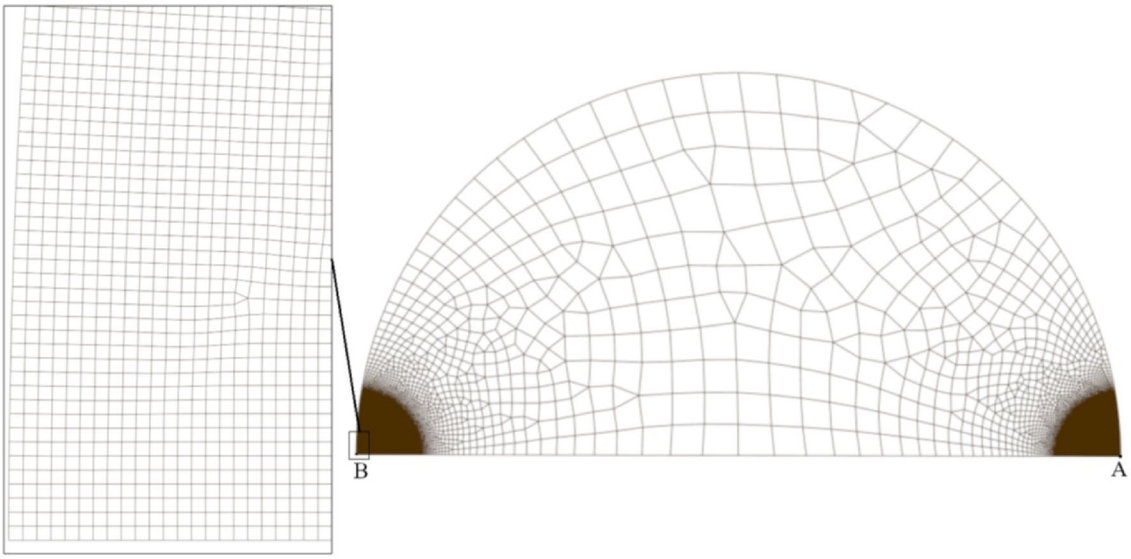

Fig. 2 Particle mesh generated in Gmsh

$$a_y = \sqrt{\delta_y R^*} \tag{4}$$

Starting from the initial element size, a convergence study was conducted to ensure proper refinement of the mesh. The convergence study goal was set to less than 1% and included the main impact quantities, such as: the maximum impact force, impact duration and rebound velocity [35]. Based on this study, the element size was set as 0.0166 mm and was obtained for the steel-steel material pair. Such a size was set for all finite elements where the distance from initial contact points A or B was smaller than 1.673 mm. This distance was obtained by multiplication of the largest contact area radius by the factor 3. This guaranteed that the contact area and the surrounding elements, where high stresses were expected, had fine discretization. Starting from the distance 1.673 mm from points A and B, the element size was gradually increased up to 1 mm. The same mesh was used for both particles.

The FEM model was built in Code_Aster version 14.6 [77]. It used solver DYNA_NON_LINE for the solution, for which the initial time step was set to 3.25 μs but was adapted automatically when the convergence criterion was not met. Discrete formulation was used to model contact. Automatic detection of the contact zone is currently not supported by Code_Aster, therefore all elements in the fine mesh area were specified for the potential contact occurrence. When the particles were made of different materials, the elements belonging to the stiffer particle were defined as 'master'. The materials were modelled as elastic – ideally plastic, according to parameters given in Table 2, and assigned to axisymmetric elements, named 'AXIS' in Code_Aster. The usage of axisymmetric elements allowed analysis of three-dimensional systems with the two-dimensional mesh shown in Fig. 2.

The FEM model was validated based on the work of Minamoto and Kawamura [75]. For this purpose, it was adjusted to the model investigated in the reference article; the mesh was scaled, and new material (steel SUJ2) was defined. Then, the impact in the adjusted system was simulated for the same impact velocities as in the reference article. The calculated values of COR are given in Fig. 3 and, as evident from this figure, they compare well with the reference. The maximum difference between them equalled 4%. Moreover, the calculated values were closer to the experimental data reported in [75], suggesting that they were more exact. This could be explained by the usage of a finer mesh (Fig. 2).

The procedure used for the calculation of COR is detailed in the next section.

3.2 Calculation of COR

As mentioned earlier, the MK and ZG contact models require a priori knowledge of COR to express the energy dissipation during impact. To obtain the necessary values, the validated FEM model described in the previous section was used to analyse impacts of two particles for all combinations of particle materials and impact velocities. The results of the analysis were then used to calculate COR for each case.

There are three definitions of COR available in the literature: kinematic, kinetic, and energetic. It can be shown that those definitions are equivalent for the central impact of smooth bodies [27]. Therefore, because of the calculation

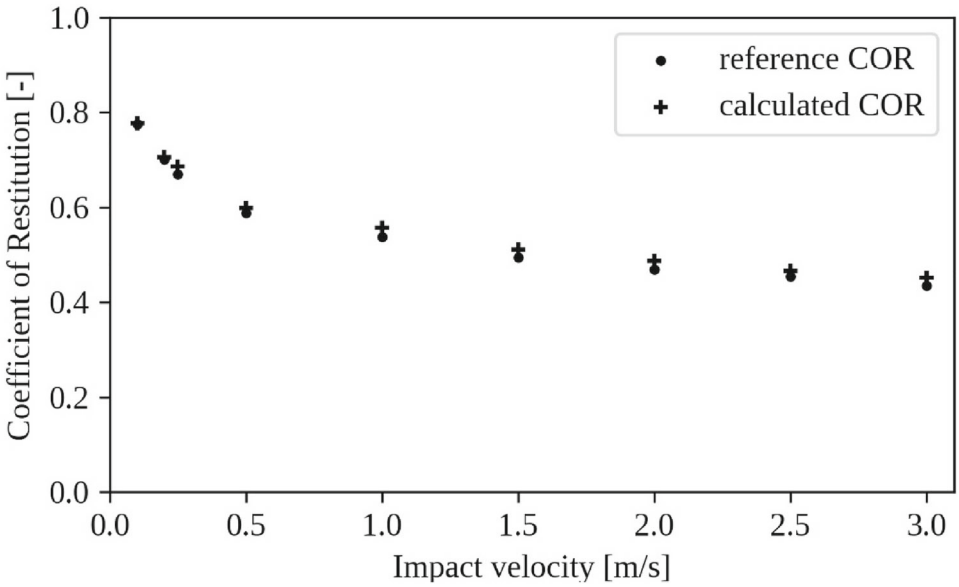

Fig. 3 Comparison of the calculated and reference COR; the reference values obtained from Fig. 7 in [75] for the elasto-plastic material model

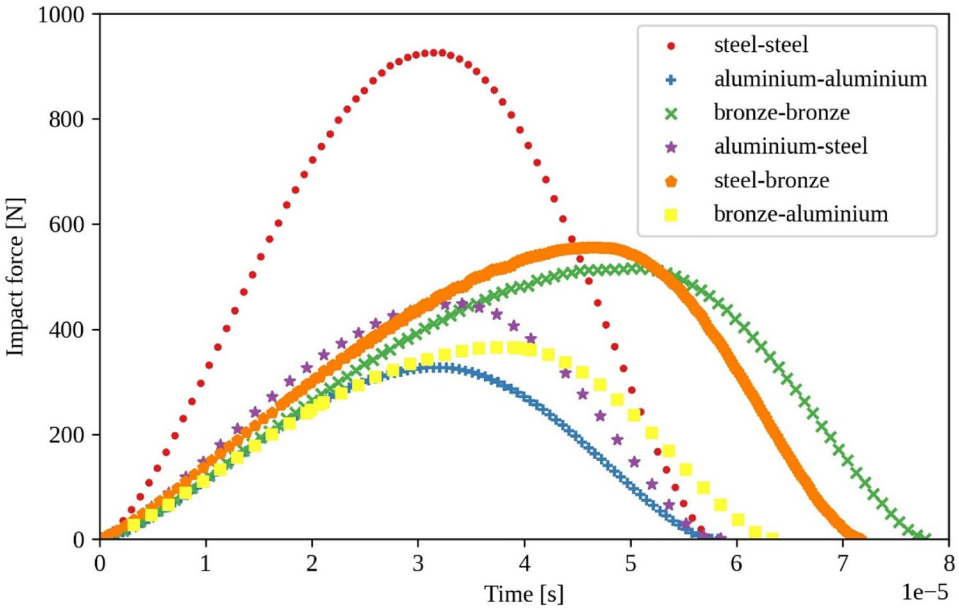

Fig. 4 Impact force as a function of time; all particle material combinations for impact velocity 1 m/s

simplicity, the kinematic definition of COR was chosen to obtain its values in the scope of this article.

The kinematic COR is defined as the ratio of the final to the initial relative, normal velocities of the impacting bodies (Eq. (5)).

$$c_r = -\frac{\dot{\delta}_f}{\dot{\delta}_0} \tag{5}$$

To calculate the final relative velocity from the FEM analysis, the velocities of all nodes for both particles were averaged for a minimum of 10 time steps after impact termination. Those 10 values were then used to calculate the final velocity of each particle by another average. Figure 5 shows as an example the velocities of two impacting bronze particles. The velocities given in each time step were obtained by averaging velocities of all particle nodes. Referring to this figure, final particle velocity was calculated as the average of its last 10 points.

The calculation of COR was performed for each of the selected particle materials and initial velocities. All the obtained results are given in Table 3. As evident from those results, the materials and velocities were chosen in a manner allowing a wide range of the COR values. The numerical simulations using the MK and ZG contact force models used values listed in Table 3.

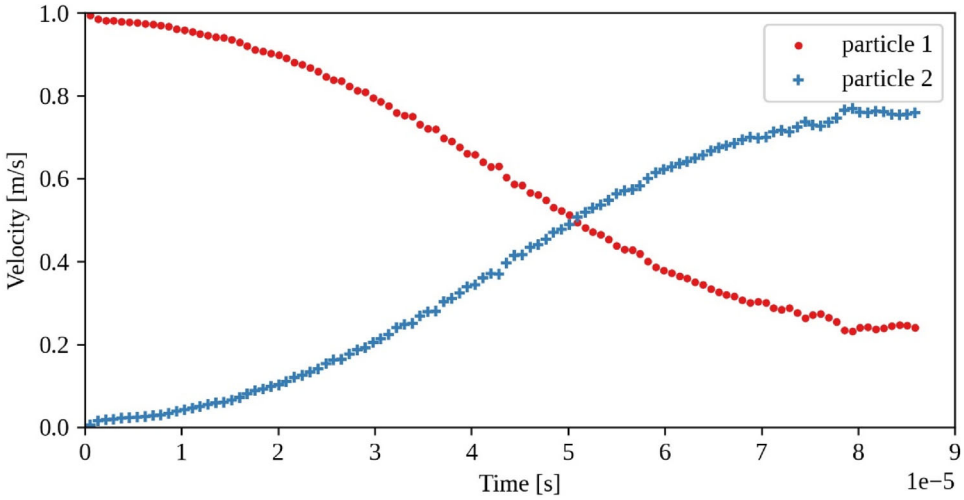

Fig. 5 Velocities of two impacting bronze particles

Table 3 Calculated values of COR for investigated particle materials and impact velocities

	0.1 m/s	1 m/s	3 m/s
Steel—steel	0.999	0.836	0.715
Aluminium – aluminium	0.998	0.803	0.680
Bronze—bronze	0.757	0.518	0.422
Aluminium – steel	0.946	0.714	0.592
Steel – bronze	0.722	0.481	0.365
Bronze—aluminium	0.874	0.629	0.499

3.3 Numerical simulations for two particles

Dissipative contact force models have been compared in many published studies. Those studies used the case of two-particle impact and were usually limited to models belonging to one group, either expressing energy dissipation by the damping factor [37, 40, 41, 44–46, 61] or plastic deformation [43, 74]. As the contact force models investigated in this article cannot be assigned to one group, it seemed reasonable to also include numerical simulation for two particles. Results obtained in such cases can also deepen the understanding of multi-zone impact cases studied further.

The simulated system consisted of two particles of masses m_1 and m_2 and radius R, as shown in Fig. 1. Assuming that the only forces acting on the particles are the impact forces, the equations describing the system can be given as follows:

$$m_1\ddot{x}_1 = -F_1 \tag{6}$$

$$m_2\ddot{x}_2 = F_1 \tag{7}$$

$$\delta = x_1 - x_2 - 2R \tag{8}$$

$$\dot{\delta} = \dot{x}_1 - \dot{x}_2 \tag{9}$$

where F_1 is the impact force described by one of the models given in Table 1 and x_1 and x_2 are coordinates giving the position of the particles. The given equations were implemented in the Python programming language using the SciPy and NumPy libraries. The integration was performed by the explicit Runge–Kutta method of order (4)5 with a time step equal 10^{-8} s.

The published review studies used various quantities, such as maximal impact force, impact duration, and indentation etc., to assess the validity of the compared contact force models. Nevertheless, this article mainly uses COR for the comparison of the selected contact force models. Such a choice was justified by several factors: COR expresses various sources of energy dissipation, it is well established by experimental settings, widely used in the literature, and allows determination of velocities of impacting bodies, which, when performed correctly, may be sufficient for the accurate simulation of a multi-body system. COR gives a number value which can be easily used for comparison purposes, but it hides various aspects of the investigated contact force model. Such aspects can be better identified when represented graphically. For this purpose, plots representing the time history of the impact forces for the compared contact force models were created. Examples of such plots are shown in Figs. 6 and 7.

4 Simultaneous multi-zone impacts – investigation methodology

Modelling simultaneous, multi-zone impacts poses several challenges. The interactions between the colliding particles often mean it is impossible to make a clear distinction

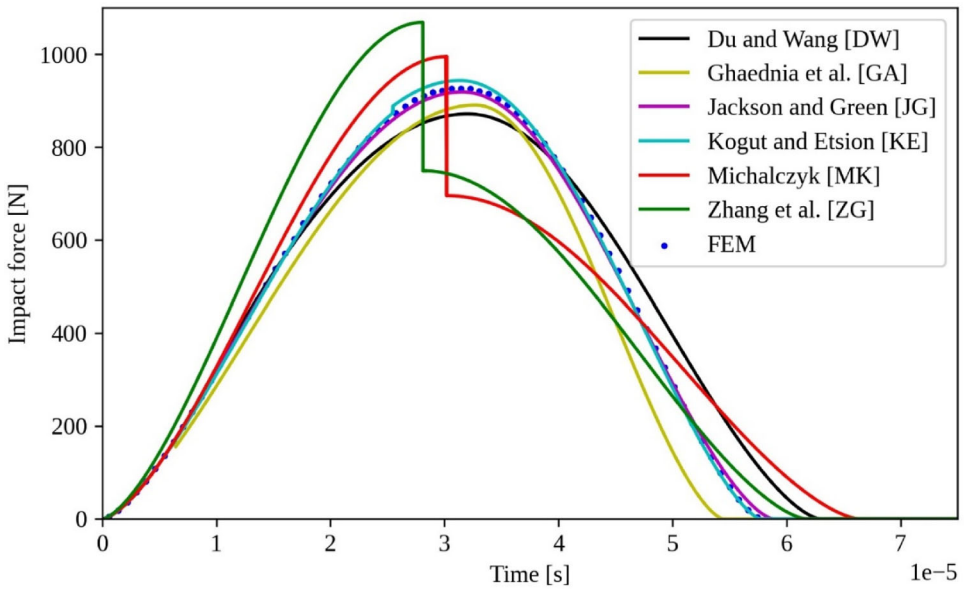

Fig. 6 Time history of the impact forces for the collision of two steel particles, initial impact velocity equal 1 m/s

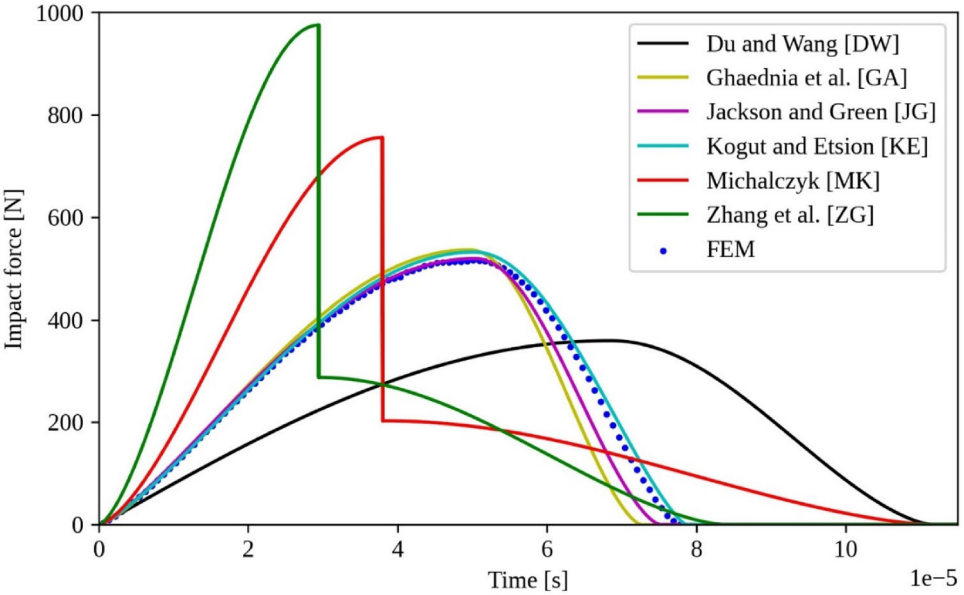

Fig. 7 Time history of the impact forces for the collision of two bronze particles, initial impact velocity equal 1 m/s

between the compression and restitution phases, i.e., the collision between two particles can switch to the compression phase before the end of the restitution phase. Moreover, the initial impact velocity can usually be determined a priori only for the initiating impact and the compliant contact force models available in the literature were developed and validated only for two-body impacts, therefore, their performance in more complex cases demands clarification.

Collinear systems of up to 6 particles were used for the purpose of the investigation. All particles except the first two were in contact before the initial impact, as schematically shown for 6 particles in Fig. 8. The maximum quantity of the particles was set based on the width of the solitary wave pulse, which was reported to approximately equal 5 particle diameters [27]. Such a choice offered a reasonably robust balance between computation cost, crucial especially for FEM analysis, and the phenomena occurring in the analysed system. The next sections will give more detailed information on the definition of numerical experiments performed in the scope of this article.

4.1 Analysed cases

The phenomena occurring during multi-zone impact depend not only on the length of the chain but also on the particle material properties. To also include this behaviour, 3 different materials were selected: steel, aluminium, and bronze. Their

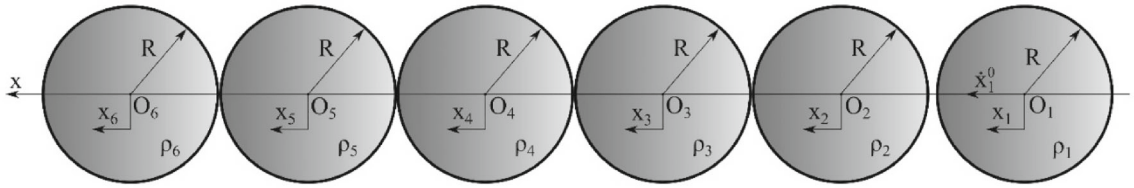

Fig. 8 Example of a collinear system consisting of 6 particles

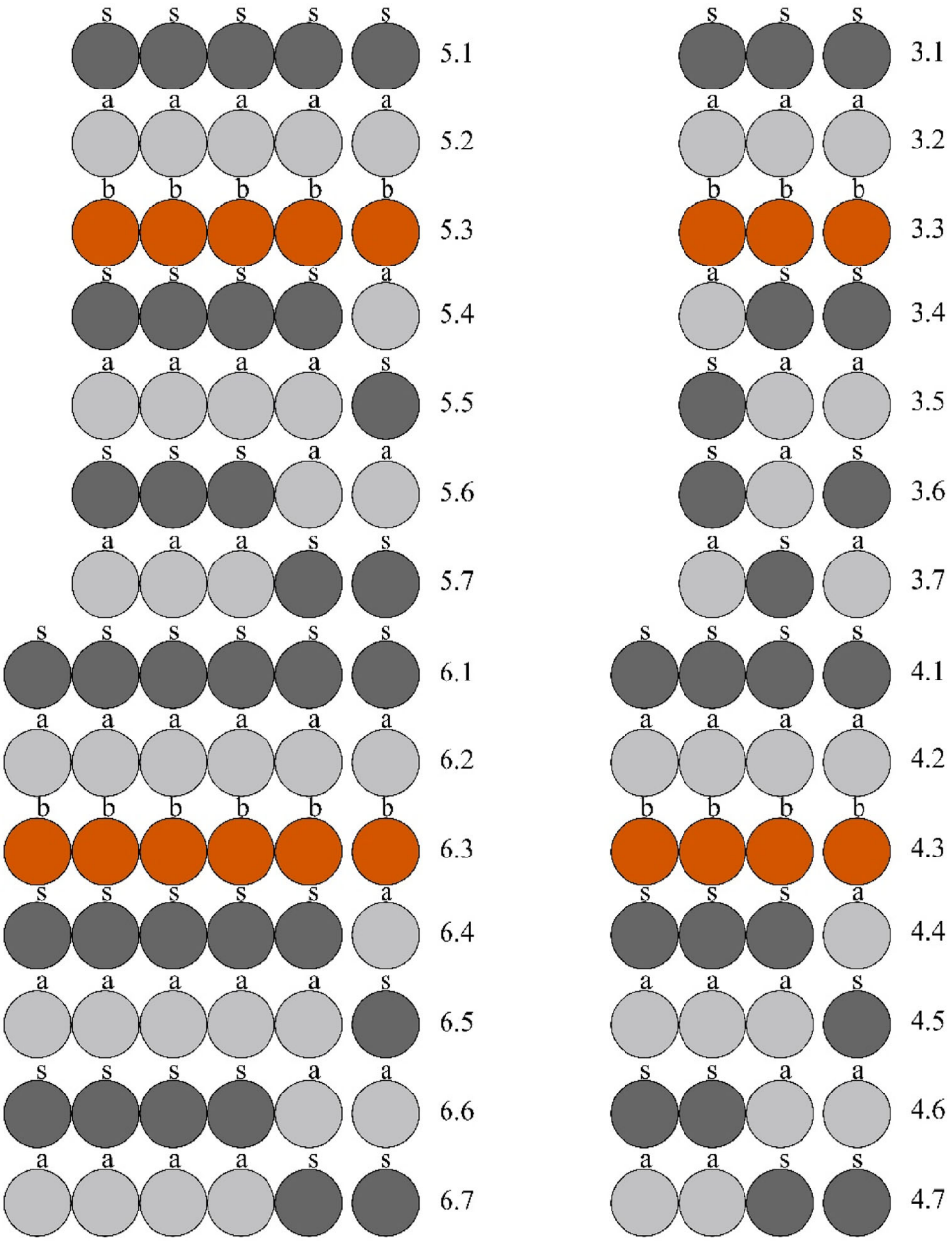

Fig. 9 Analysed particle sequences (a – aluminium, b – bronze, s – steel, material properties are given in Table 2)

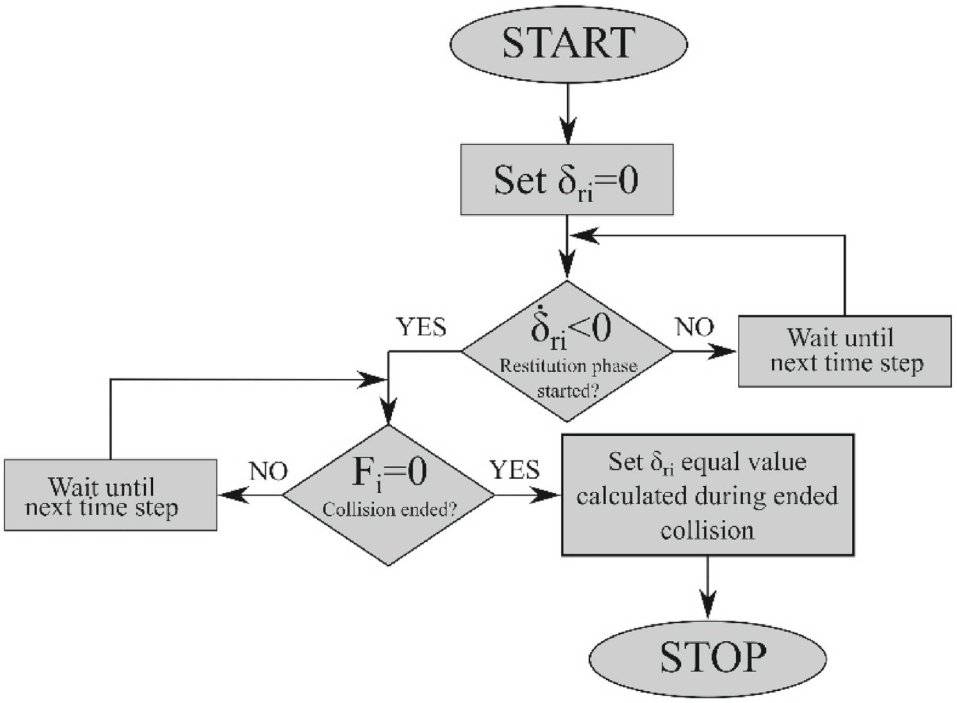

Fig. 10 Algorithm for determining residual deformation

properties were given in Table 2. They differ in Young modulus and yield strength. Particle chains not only consisted of particles made from the same material, but additional cases were also added. For clarity, all of them are presented graphically in Fig. 9. Each of the analysed cases had an assigned number identifying it. The first number gives the quantity of particles, while the second identifies the sequence of materials. For example, number 5.2 identifies a case with 5 particles, all of which were made from aluminium. Those numbers will be used further for referencing each case. Additionally, 3 different velocities were analysed to cover a wide range of plastic deformation, which corresponds to different values of COR or energy dissipation. Those velocities equalled 0.1 m/s, 1 m/s and 3 m/s.

4.2 Numerical model

The equations governing the system were dependent on the number of particles. With an increasing number of particles, the number of degrees of freedom increased, requiring more equations for system description. To avoid repetition of very similar equation systems, the used equations were given in a generalised form, in which equations for a particular system can be achieved by setting the index "n" equal to the number of particles in the system.

$$m_1\ddot{x}_1 = -F_1 \tag{10}$$

$$m_i\ddot{x}_i = -F_{i-1} + F_i \tag{11}$$

$$m_n\ddot{x}_n = F_n \tag{12}$$

$$\delta_1 = x_1 - x_2 - \delta_{r1} \tag{13}$$

$$\delta_i = x_i - x_{i+1} - \delta_{ri} \tag{14}$$

$$\dot{\delta}_1 = \dot{x}_1 - \dot{x}_2 \tag{15}$$

$$\dot{\delta}_i = \dot{x}_i - \dot{x}_{i+1} \tag{16}$$

where: m – mass of the particle, x – coordinate describing the position of the particle, R – particle radius, F – impact force described by one of the contact models given in Table 1, δ – local particle deformation, $\dot{\delta}$ – relative velocity of two particles, δ_r – residual deformation from the previous collision between particles i and i + 1, n – number of particles, n ϵ [3, 6], i = 2.. n-1.

The residual deformation introduced in Eqs. (13) and (14) stored information about the permanent deformation of two adjacent particles. Its value was equal 0 for the duration of the first collision between two particular particles, because for such a case the residual deformation was handled by the contact force model. Exceptions to that were the MK and ZG models, for which δ_r was always equal 0. An algorithm presented in Fig. 10 gives more details about the handling of δ_r in the numerical simulations.

The introduction of the residual deformation δ_r was based on the results obtained from FEM analysis, which showed

Table 4 Benchmark velocity indicator (BVI) for the chain of 5 particles and 3 investigated impact velocities given with the reference value obtained by the FEM analysis. The cell colour represents error level >25%, 20-25%, 15-20%, 10-15%, 5-10%, 1-5%, <1%

	DW	GA	JG	KE	MK	ZG	FEM
5.1.1	0.9888	0.9888	0.9888	0.9888	0.987	0.9889	0.9892
5.1.3	0.8501	0.5415	0.7568	0.7689	0.7316	0.7332	0.7577
5.1.7	0.6695	0.3871	0.5949	0.6138	0.5883	0.5934	0.605
5.2.1	0.9888	0.9613	0.9793	0.9994	0.9852	0.9871	0.9872
5.2.3	0.7845	0.4927	0.7145	0.7274	0.688	0.6903	0.7146
5.2.7	0.6175	0.3607	0.5524	0.5806	0.5516	0.5646	0.5705
5.3.1	0.7147	0.4281	0.6487	0.6596	0.6317	0.6361	0.6578
5.3.3	0.3273	0.2938	0.3522	0.4306	0.4069	0.4591	0.4039
5.3.7	0.3545	0.2862	0.2616	0.3592	0.3932	0.4149	0.3162
5.4.1	0.5119	0.4659	0.496	0.4969	0.4973	0.4988	0.4996
5.4.3	0.4351	0.3015	0.3923	0.399	0.3482	0.3512	0.4013
5.4.7	0.3522	0.2265	0.3144	0.3332	0.2735	0.279	0.3266
5.5.1	1.5381	1.3781	1.4706	1.484	1.5056	1.507	1.481
5.5.3	1.1988	0.6469	1.1427	1.1563	1.057	1.0639	1.0156
5.5.7	1.0427	0.754	0.9869	1.018	0.9093	0.9215	0.8076
5.6.1	0.5288	0.4804	0.5127	0.5153	0.5143	0.5165	0.517
5.6.3	0.4255	0.2804	0.3906	0.3913	0.3619	0.3665	0.3932
5.6.7	0.3357	0.2135	0.3019	0.3229	0.288	0.2959	0.3143
5.7.1	1.51	1.387	1.4618	1.4722	1.4746	1.4769	1.4744
5.7.3	1.1685	0.8334	1.097	1.1164	1.0297	1.0385	1.0536
5.7.7	0.9545	0.6758	0.9072	0.9461	0.8676	0.8859	0.8349

in some cases the occurrence of a second collision between adjacent particles. Moreover, the particles were permanently deformed during FEM analysis. If similar behaviour had not been implemented in the numerical model it could have resulted in collisions, which should not take place. Such a situation would increase the differences between the reference FEM analysis and investigated contact force models.

It should be noted that the analysed contact force models were developed for single loading and unloading. Although in the investigated systems that was not always the case, there were no alterations of the models, except the introduction of residual deformation in Eqs. (13) and (14). This problem was outside the scope of this article and will be addressed in future studies.

Equations (10)–(16) were numerically solved with the help of scripts written in Python 3. Those scripts utilized the libraries: SciPy, NumPy, and Matplotlib. For the solution of second-order ordinary equations, the explicit Runge–Kutta method of order (4)5 with a time step equal 10^{-8} s was used. The duration of each simulation corresponded to the time of the FEM analysis as given in Table 11.

4.3 FEM analysis

The FEM model was built in Code_Aster version 14.6 [77]. Its definition was analogous to the model described in Sect. 3.1, with the difference in the quantity of particles having an initial velocity equal to 0. Each of the particles used in the simulation had the same mesh. This was achieved by assembling the particle chain from the same mesh and then translating particles by the distance equal to the particle diameter. At the start of the simulation, the impacting particle was not in contact with the next particles, while all the other particles were in contact.

Table 5 Benchmark velocity indicator (BVI) for the chain of 4 particles and 3 investigated impact velocities given with the reference value obtained by the FEM analysis. The cell colour represents error level >25%, 20-25%, 15-20%, 10-15%, 5-10%, 1-5%, <1%

	DW	GA	JG	KE	MK	ZG	FEM
4.1.1	0.991	0.991	0.991	0.991	0.9896	0.9911	0.9914
4.1.3	0.8745	0.6117	0.8013	0.8125	0.7737	0.7863	0.8052
4.1.7	0.7229	0.4728	0.6614	0.6794	0.658	0.6629	0.6707
4.2.1	0.991	0.9673	0.983	0.9982	0.9982	0.9897	0.9897
4.2.3	0.8115	0.5679	0.7654	0.777	0.7302	0.75	0.77
4.2.7	0.6777	0.4493	0.6235	0.6507	0.6241	0.6329	0.6371
4.3.1	0.7618	0.5097	0.7088	0.7184	0.6992	0.7026	0.7192
4.3.3	0.5182	0.3918	0.437	0.5172	0.516	0.5322	0.4887
4.3.7	0.4394	0.3849	0.3463	0.4506	0.4616	0.4835	0.4022
4.4.1	0.5134	0.4673	0.4974	0.4983	0.4989	0.5002	0.5011
4.4.3	0.4366	0.3244	0.4046	0.4113	0.3742	0.3774	0.4145
4.4.7	0.3668	0.2622	0.3369	0.3556	0.3074	0.3139	0.3489
4.5.1	1.5338	1.3855	1.4737	1.4843	1.4996	1.5012	1.4845
4.5.3	1.2264	0.7665	1.1745	1.1886	1.1281	1.1372	1.108
4.5.7	1.0643	0.8693	1.0352	1.0769	0.9918	1.0044	0.9106
4.6.1	0.5309	0.4825	0.5149	0.5174	0.5165	0.5185	0.5192
4.6.3	0.4268	0.3018	0.4036	0.4039	0.3889	0.394	0.4064
4.6.7	0.349	0.2463	0.3238	0.3445	0.3226	0.3318	0.3379
4.7.1	1.4953	1.3769	1.4519	1.4588	1.4556	1.4577	1.4646
4.7.3	1.2006	0.8674	1.1238	1.1445	1.0942	1.1034	1.1247
4.7.7	1.0035	0.7301	0.9343	0.9785	0.9411	0.9596	0.927

The initial simulation time step was equal to 3.25 μs. It was automatically adjusted by the solver when the convergence criteria were not met, which was mainly influenced by the initial impact velocity and the level of plastic deformation occurring in the contact area. The simulation time was varied depending on the particle quantity, initial impact velocity, computational cost, and a requirement that each particle must take part in the collision. As the main purpose of the conducted numerical experiment was to investigate the performance of selected contact force models in modelling simultaneous, multi-point impact, the absolute value of simulation time was of secondary importance if the duration of the numerical simulation and FEM analysis was the same. The simulation time for each of the particle sequences and velocities is listed in Table 11.

5 Results and discussion

Most studies focus on predicting the post impact velocities of colliding particles. An accurate prediction of body velocity is crucial in multi-body and Discrete Element Method (DEM) simulations. Therefore, for this study, velocity was selected as the main benchmark quantity for the comparison of the chosen contact force models. As the investigated systems consisted of 3 to 6 particles, they have been treated as a "black box" with input defined as an initial velocity of the particle initiating impact and the output being the post impact velocity of the last particle in the chain. Those two values were used to define the *benchmark velocity indicator (BVI)* given by the following equation:

$$BVI = \frac{\dot{x}_n^f}{\dot{x}_1^i} \tag{17}$$

Table 6 Benchmark velocity indicator (BVI) for the chain of 3 particles and 3 investigated impact velocities given with the reference value obtained by the FEM analysis. The cell colour represents error level >25%, 20-25%, 15-20%, 10-15%, 5-10%, 1-5%, <1%

	DW	GA	JG	KE	MK	ZG	FEM
3.1.1	0.9945	0.9945	0.9945	0.9945	0.9936	0.9946	0.9951
3.1.3	0.9075	0.7016	0.8532	0.863	0.8462	0.8472	0.8555
3.1.7	0.789	0.5893	0.7433	0.759	0.7461	0.7502	0.7562
3.2.1	0.9945	0.9755	0.9882	0.9984	0.9926	0.9937	0.9923
3.2.3	0.8655	0.6662	0.8255	0.8334	0.8181	0.8196	0.828
3.2.7	0.7531	0.5706	0.7125	0.7366	0.7188	0.7245	0.7233
3.3.1	0.8196	0.619	0.7813	0.7891	0.7799	0.7826	0.7892
3.3.3	0.623	0.5261	0.5541	0.6292	0.6071	0.6234	0.6067
3.3.7	0.4925	0.5197	0.4706	0.573	0.5305	0.58	0.5232
3.4.1	1.424	1.3082	1.3848	1.3874	1.3873	1.3859	1.3941
3.4.3	1.1904	0.9129	1.1307	1.1528	1.127	1.043	1.1532
3.4.7	1.034	0.8038	0.9696	1.0216	0.9818	0.9865	1.0157
3.5.1	0.547	0.4949	0.5293	0.5323	0.5333	0.5343	0.5338
3.5.3	0.4463	0.3337	0.4269	0.4285	0.4413	0.443	0.4282
3.5.7	0.386	0.296	0.3582	0.381	0.3983	0.4022	0.3745
3.6.1	0.886	0.7757	0.8458	0.8483	0.8741	0.8743	0.8449
3.6.3	0.762	0.6449	0.7129	0.731	0.7785	0.7839	0.6775
3.6.7	0.7121	0.6372	0.665	0.6884	0.7342	0.7411	0.6578
3.7.1	0.7518	0.6699	0.7226	0.726	0.7118	0.7123	0.7304
3.7.3	0.5904	0.4599	0.5721	0.582	0.5481	0.5534	0.5881
3.7.7	0.5135	0.4129	0.4866	0.5191	0.474	0.4831	0.5178

where: $\dot{x}_1^i$ is the initial velocity of the particle initiating impact and $\dot{x}_n^f$ is the velocity of the particle last in the sequence at the simulation end.

The BVI defined in such a way describes the ability of the given contact force model to predict the collision force impulse, which is an integral of contact force over time. Consequently, a contact force model that accurately predicts the collision force and duration may have the same BVI as the model, which underestimates the contact force and overestimates the collision duration. To minimize this drawback, the simulation time was varied (as given in Table 11). This, combined with a high number of simulations, should guarantee that the conclusions were reasonable.

Tables 4, 5, 6 and 7 summarize the BVI calculated in each simulation experiment. The numbers given in the first column identify the particle sequence and the initial velocity of the particle initiating impact. The first two numbers relate to the sequences shown in Fig. 9 and the last number can take three values: 1, 3 or 7 corresponding to the velocities 0.1 m/s, 1 m/s and 3 m/s, respectively. To allow a better visual comparison between the analysed contact force models, each BVI value was coloured. This error was calculated taking the BVI values obtained by FEM simulations as the reference (given in the last columns of Tables 4, 5, 6 and 7).

The analysis of the results presented in Tables 4, 5, 6 and 7 lead to the conclusion that the KE and JG models allow the lowest levels of error. Considering their simplicity, the MK and ZG models showed unexpectedly good results. However, it should be remarked that, for those models, the pre-restitution coefficient was defined based on the results given in Tables 8, 9 and 10 and they showed good agreement of pre- and post-restitution coefficients. Nevertheless, the applied COR was chosen based on the velocity of the initiating impact and was the same for all impacts in the given

Table 7 Benchmark velocity indicator (BVI) for the chain of 6 particles and 3 investigated impact velocities given with the reference value obtained by the FEM analysis. The cell colour represents error level >25%, 20-25%, 15-20%, 10-15%, 5-10%, 1-5%, <1%

	DW	GA	JG	KE	MK	ZG	FEM
6.1.1	0.9875	0.9875	0.9875	0.9875	0.9853	0.9877	0.9876
6.1.3	0.8278	0.4853	0.7178	0.7302	0.6844	0.6862	0.7232
6.1.7	0.625	0.3229	0.5395	0.5585	0.5357	0.5403	0.5496
6.2.1	0.9875	0.9566	0.9767	1.0014	0.9831	0.9855	0.9857
6.2.3	0.7532	0.4337	0.6703	0.6856	0.6358	0.6384	0.6742
6.2.7	0.5541	0.2951	0.4941	0.522	0.479	0.5117	0.5087
6.3.1	0.6718	0.3658	0.5967	0.6095	0.5591	0.5805	0.6066
6.3.3	0.3772	0.222	0.289	0.3623	0.3903	0.4055	0.3353
6.3.7	0.2371	0.2134	0.2021	0.2897	0.3225	0.362	0.2476
6.4.1	0.5111	0.4651	0.4952	0.496	0.4963	0.498	0.4988
6.4.3	0.4342	0.282	0.3815	0.3882	0.3253	0.3281	0.3915
6.4.7	0.3396	0.1987	0.295	0.3126	0.245	0.2515	0.3046
6.5.1	1.5406	1.3666	1.4651	1.4812	1.5089	1.5104	1.4776
6.5.3	1.1764	0.555	1.1139	1.1279	0.9946	0.9993	0.9476
6.5.7	0.9859	0.6826	0.961	0.9961	0.843	0.852	0.7184
6.6.1	0.5275	0.4792	0.5114	0.514	0.5129	0.5154	0.5158
6.6.3	0.4247	0.2627	0.3796	0.3805	0.3381	0.3423	0.3843
6.6.7	0.3246	0.1881	0.2835	0.3031	0.2621	0.2683	0.2939
6.7.1	1.5194	1.385	1.4644	1.4777	1.4859	1.4883	1.4759
6.7.3	1.1475	0.7967	1.0695	1.0889	0.9721	0.9799	0.9834
6.7.7	0.9335	0.6408	0.8675	0.8997	0.7981	0.8156	0.7384

Table 8 COR obtained for contact models from numerical simulation for impact velocity 1 m/s

	[DW]	[GA]	[JG]	[KE]	[MK]	[ZG]	FEM
Steel—steel	0.895	0.644	0.834	0.849	0.836	0.837	0.836
Aluminium – aluminium	0.845	0.600	0.800	0.809	0.803	0.805	0.803
Bronze—bronze	0.538	0.429	0.447	0.559	0.518	0.543	0.518
Aluminium – steel	0.722	0.492	0.679	0.706	0.714	0.719	0.714
Steel – bronze	0.492	0.423	0.387	0.522	0.481	0.512	0.481
Bronze—aluminium	0.609	0.442	0.540	0.615	0.629	0.640	0.629

experiment. This was a necessary simplification as only the velocity of the particle initiating impact was known a priori. The worst results were obtained for the GE model. This model seems to have a tendency to shorten the intensity and the duration of the collision restitution phase, which amplifies through the next impacts and causes quick accumulation of the error, not seen in two-particle impacts. Therefore, although this model has a similar definition in the compression phase to the JG model, it produced the highest levels of error. The DW model, on the contrary, extends the duration of the impact. Its error was therefore sensible for the chosen

Table 9 COR obtained for contact models from numerical simulation for impact velocity 3 m/s

	[DW]	[GA]	[JG]	[KE]	[MK]	[ZG]	FEM
Steel—steel	0.751	0.505	0.698	0.721	0.715	0.720	0.715
Aluminium–aluminium	0.706	0.482	0.659	0.693	0.680	0.687	0.680
Bronze—bronze	0.448	0.418	0.325	0.485	0.422	0.464	0.422
Aluminium – steel	0.602	0.441	0.531	0.611	0.592	0.607	0.592
Steel – bronze	0.410	0.416	0.276	0.454	0.365	0.420	0.365
Bronze—aluminium	0.507	0.424	0.404	0.534	0.499	0.527	0.499

Table 10 COR obtained for contact models from numerical simulation for impact velocity 0.1 m/s

	[DW]	[GA]	[JG]	[KE]	[MK]	[ZG]	FEM
Steel—steel	1.000	1.000	1.000	1.000	0.999	1.000	0.999
Aluminium–aluminium	1.000	0.974	0.991	1.000	0.998	0.999	0.998
Bronze—bronze	0.789	0.541	0.746	0.757	0.757	0.760	0.757
Aluminium – steel	0.998	0.812	0.937	0.937	0.946	0.947	0.946
Steel – bronze	0.722	0.491	0.676	0.704	0.722	0.727	0.722
Bronze—aluminium	0.887	0.644	0.834	0.849	0.874	0.875	0.874

Table 11 FEM simulation time given in μs for all particle combination variants

	0.1 m/s	1 m/s	3 m/s		0.1 m/s	1 m/s	3 m/s
6.1	300	300	300	4.1	225	125	150
6.2	350	300	175	4.2	225	125	120
6.3	400	600	300	4.3	350	300	300
6.4	350	300	200	4.4	225	180	130
6.5	350	300	300	4.5	300	180	250
6.6	350	300	300	4.6	300	160	180
6.7	350	300	300	4.7	300	180	150
5.1	300	200	175	3.1	200	130	125
5.2	300	200	150	3.2	200	130	125
5.3	350	250	400	3.3	250	175	140
5.4	350	200	190	3.4	220	160	110
5.5	350	200	190	3.5	220	160	130
5.6	350	200	185	3.6	250	130	140
5.7	350	180	250	3.7	250	110	130

simulation time (it showed better results if the chosen simulation time was much longer than the duration of impact resulting from FEM analysis) and showed error levels somewhat worse than the MK and ZG models.

The error levels obtained for each model in all simulations are illustrated in Fig. 11. It can be easily seen that the error drops with smaller values of the initiating velocity and increases with the number of particles included in the simulation experiment. Those results seem to be reasonable and confirm the overall correctness of the conducted simulations.

The ability to predict the BVI by the analysed models depended on the particle configuration (various materials as shown in Fig. 9) and the initial velocity of the particle initiating impact. The mentioned factors determined the level of the particle plastic deformation during collision. Higher velocity increased impact intensity causing bigger local deformations, which included plastic deformation. The yield strength for each material determined the moment at which plastic deformation started, causing significant differences for steel and bronze, for example. Consequently, it may seem that the

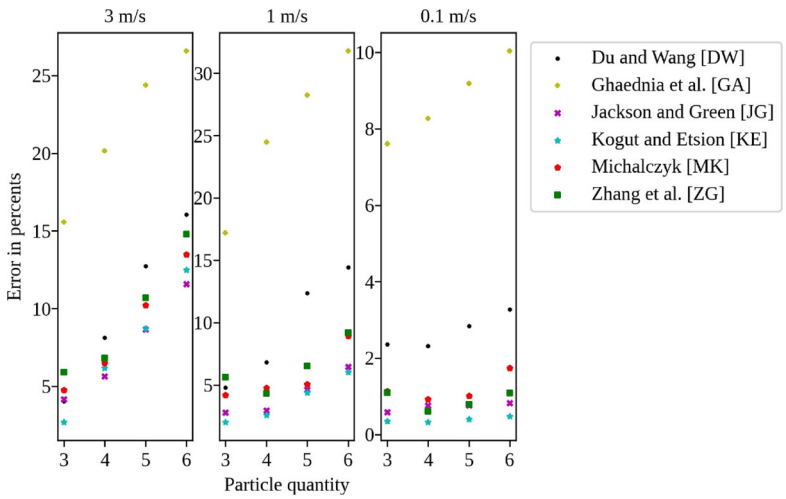

Fig. 11 Error levels for all investigated contact force models

obtained errors could be attributed to the ability to predict the plastic deformation. Although such a statement was essentially justified, the errors calculated for two-particle impacts, reported in Sect. 3, indicated that this should not have been the only source of the error.

To further investigate this problem, impact force plots were analysed. Examples of such plots are shown in Figs. 12, 13, 14 and 15. Analysis of those plots showed that, during the simultaneous, multi-zone collisions, the restitution phase can change directly into a compression phase, but the investigated contact force models were developed for simple impact cases, where the restitution phase is followed by the impact end. As a consequence of that, when the change from the restitution phase to compression phase occurs, the models switch the mathematical equation describing contact force, which in turn causes discontinuities visible in the impact force plots. This was especially visible for the MK and ZG models because the equations of those models have significant discontinuity between the compression and restitution phases. In extreme cases, shown in Figs. 12 and 13 for cases 6.3.3 and 6.3.7, the changes between phases were very frequent, causing many changes in impact force and making the plot difficult to comprehend. It may be reasonable to suppose that the calculated errors can be reduced by improvement of the contact force models through adding the ability to keep continuity of the impact force when the change from the restitution to compression phases occurs.

Figures 16 and 17 demonstrate changes in the velocities of particles 1 and 6 induced by impacts in the same numerical experiments for which impact forces were shown in Figs. 12, 13, 14 and 15. The presented time history of the particles' velocities provides detailed insight into the development of differences between the reference FEM data and the investigated contact force models. As evident from both figures, the curves representing the models with lowest errors (KE and JG) follow the reference FEM points closely, whereas the worst model (GA) protrudes from them quickly. The value of BVI captures the velocity state from the end of the calculated time history (e.g., the last points in Fig. 16 for each contact force model), which should guarantee a reasonable comparison as the differences between the reference FEM data and compared contact force models show no significant changes.

The contact force discontinuity problem can also be observed in force–displacement relations. Figure 18 contains such relations for the experiment (5.7.3), selected as an example. Four impacts occur during this experiment. The first (between particles 1 and 2, made of steel) and the last (between particles 4 and 5, made of aluminium) follow the scheme of simple, two-body impact. In this case, the compression phase is directly followed by the restitution phase, at the end of which the impact ends leaving permanent (residual) deformation. As illustrated by Fig. 18, all the analysed contact force models essentially follow this scheme, although they differentiate noticeably from the FEM results. On the contrary, the impacts between particles 2 and 3 (made of steel and aluminium, respectively) and between particles 3 and 4 (made of aluminium) demonstrate more complex behaviour. The FEM plots for these impacts reveal the switch to the compression phase occurring during the restitution phase. In the course of the switch, the FEM model maintains the force continuity and shows that the newly started compression phase does not follow the unloading curve. Moreover, the contact stiffness during the first and second compression phases clearly differs and, at least in the analysed cases, the second compression does not cause additional plastic deformation, although this should be contributed to the lower intensity of the second compression phase. None of the analysed contact force models was able to demonstrate this behaviour. Inspection of the relevant plots in Fig. 18 indicates that the analysed models switch back to the first compression curve,

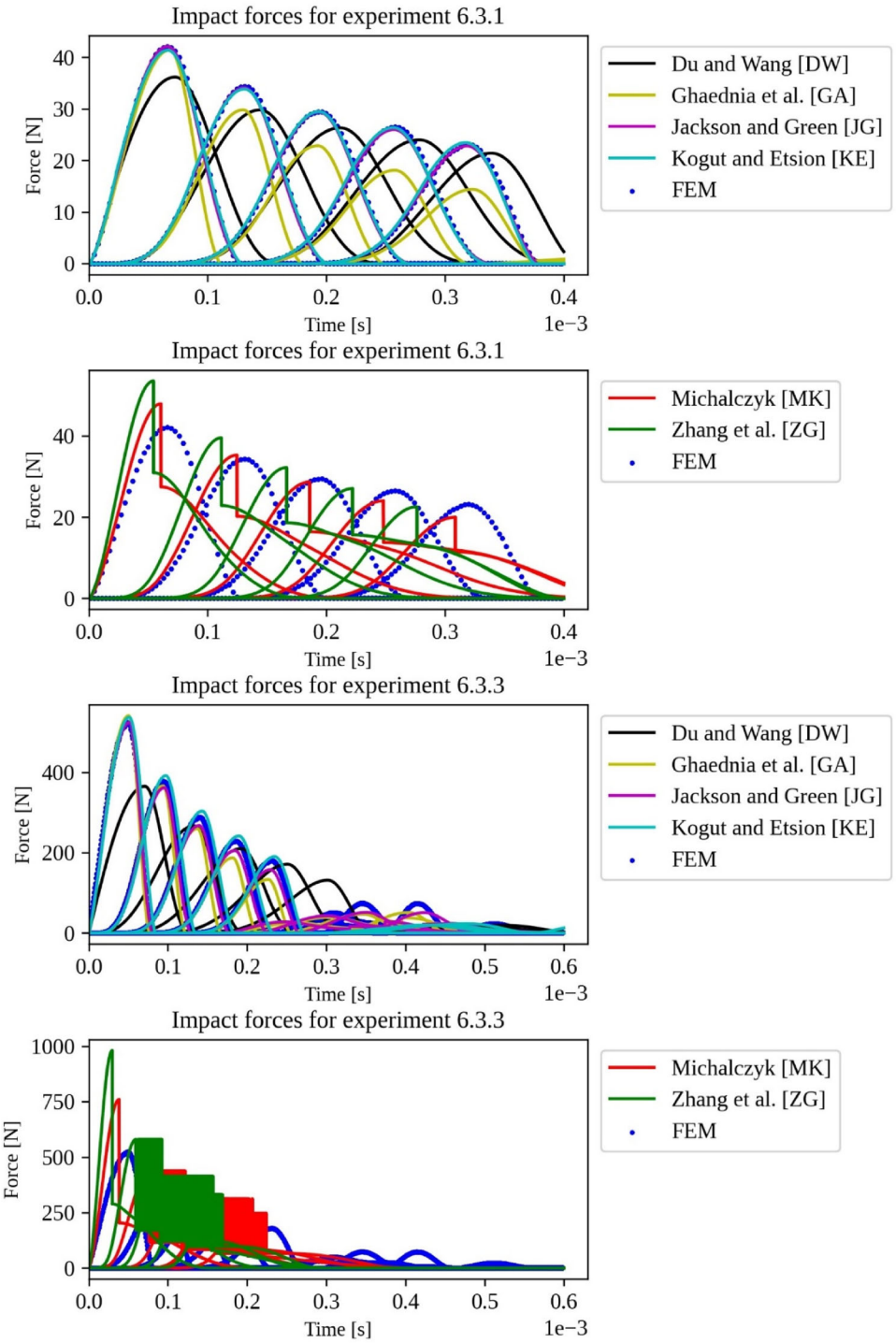

Fig. 12 Impact forces for numerical experiments in a 6 particle system part 1; for transparency the DW, GA, JG, KE, MK, and ZG models were separated

causing discontinuity in the contact force. This accounts for significant errors reported in Tables 4, 5, 6 and 7.

The conducted numerical experiments revealed phenomena occurring during simultaneous, multi-zone impacts, which are not present in simple, two-particle systems. The inner mechanism of this phenomenon can be related to the interplay of impacting particles. The impact force impulse initiated by the first particle travels through the particle chain and can be interpreted as a wave that bounces back from the last particle and interferes with itself. This may cause a sudden change in the impact state, i.e., direct switch from the restitution to compression phases, or cause subsequent impacts along the same impact normal. The present study showed that both phenomena are insufficiently represented

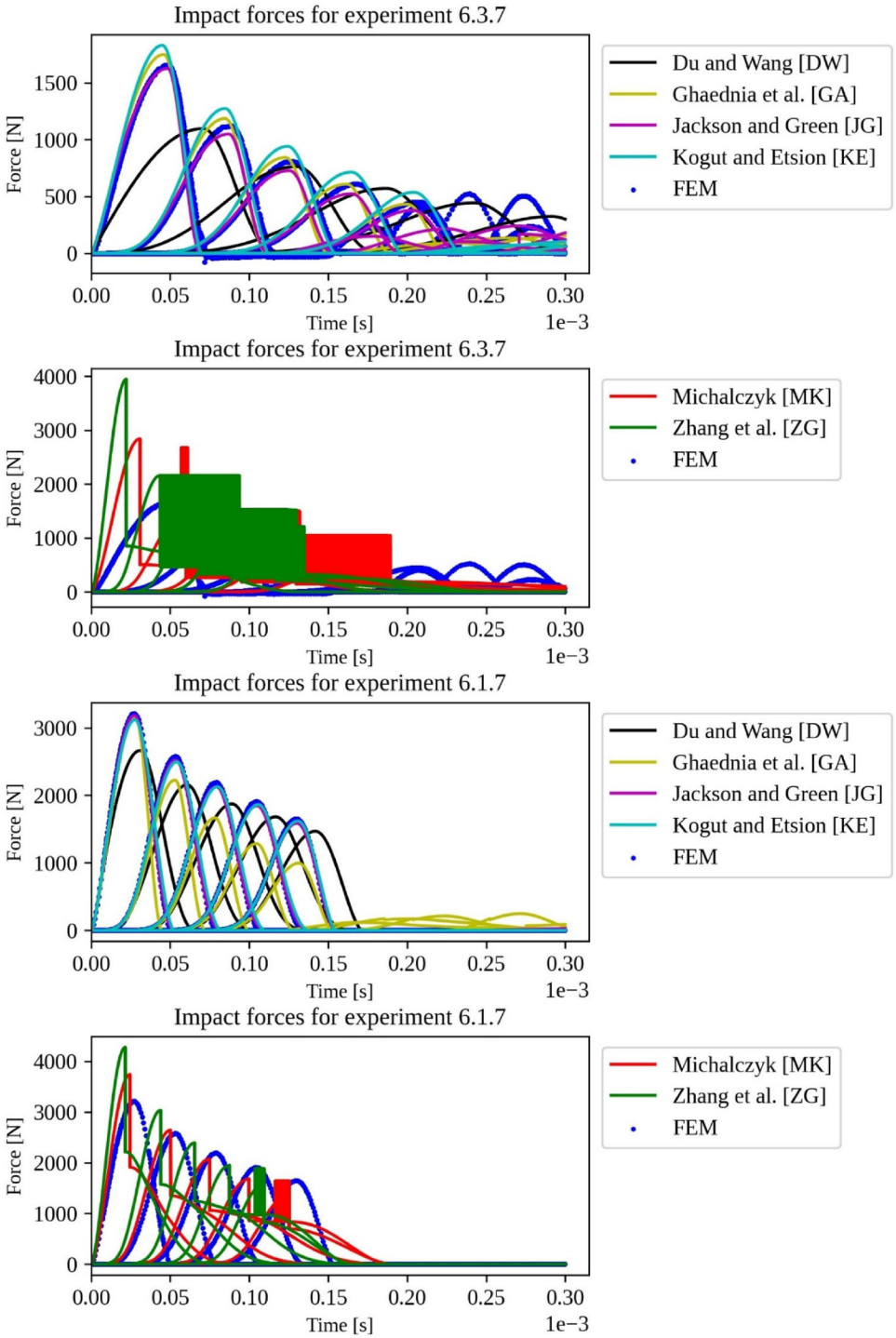

Fig. 13 Impact forces for numerical experiments in a 6 particle system part 2; for transparency the DW, GA, JG, KE, MK and ZG models were separated

by the published contact force models. This is evident from Fig. 11, which illustrates error levels for each experiment. The revealed phenomena have a negligible influence when the impact is predominantly elastic, as the impact force in this case approximately follows the same curve (there is no energy dissipation) The low error levels obtained for impacts with initiating velocity of 0.1 m/s confirm this. The error level increases significantly with increasing initiating velocity because a higher impact intensity causes larger plastic deformations, and effects of the direct switch from the restitution phase to the compression phase become significant.

Except for the initiating impact velocity, the described phenomena may also be influenced by the composition of

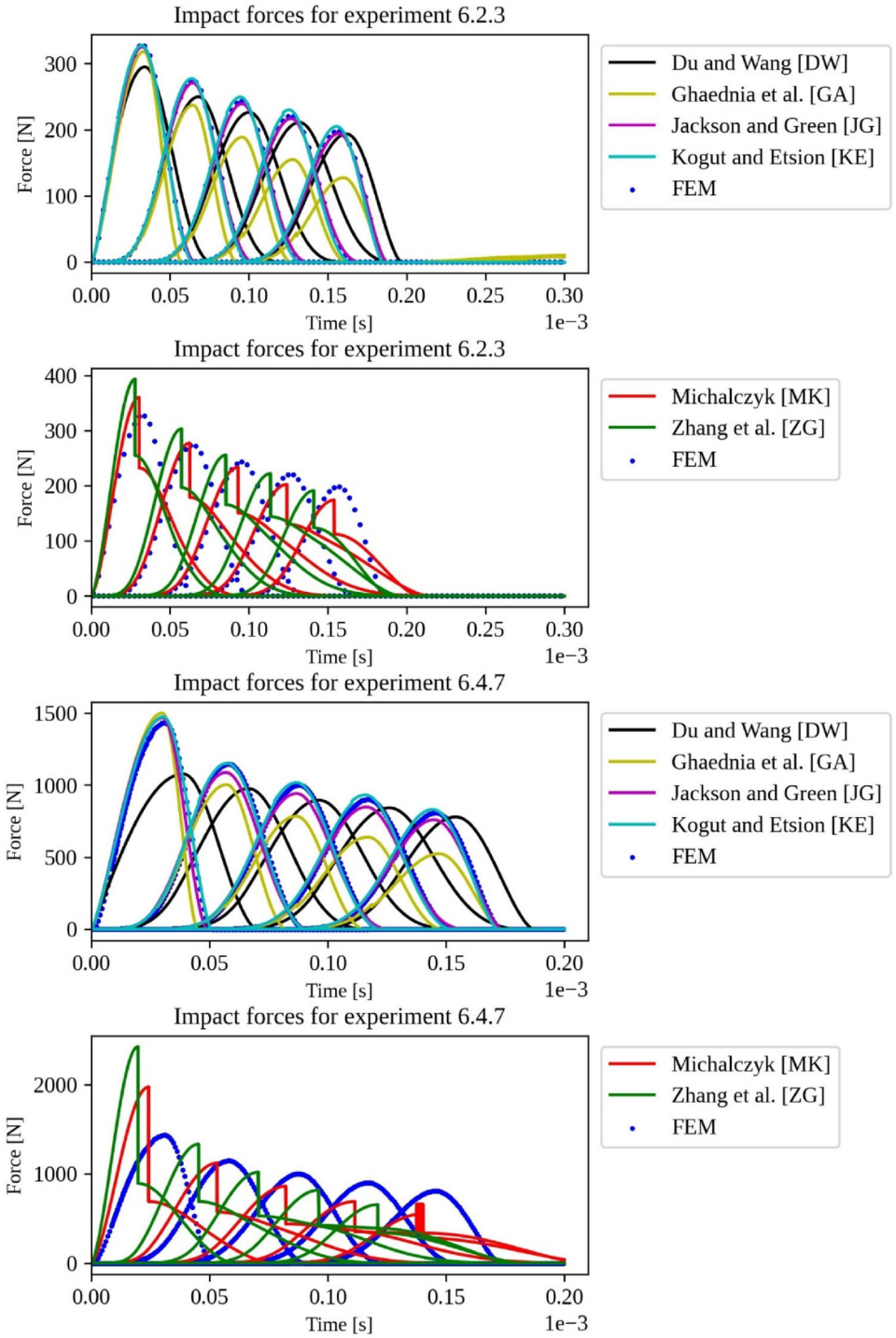

Fig. 14 Impact forces for numerical experiments in a 6 particle system part 3; for transparency the DW, GA, JG, KE, MK and ZG models were separated

the particle chain. If the particles are made of different materials, the contact stiffness varies, and with it the impact time is shortened or elongated (increase in the contact stiffness shortens impact duration). Furthermore, the particles made of different materials have differing masses (assuming the same size) which results in distinct dynamic behaviour due to other inertia. The lower mass particles react more rapidly on the acting forces, transferring the impact impulse faster to subsequent particles. Therefore, both factors influence the speed with which the impact wave travels through the particle chain and, consequently, affect the phenomena occurring during the multi-zone, simultaneous impact. Similar effects should also be seen in particle chains composed of particles made of the same material but with varying sizes, although

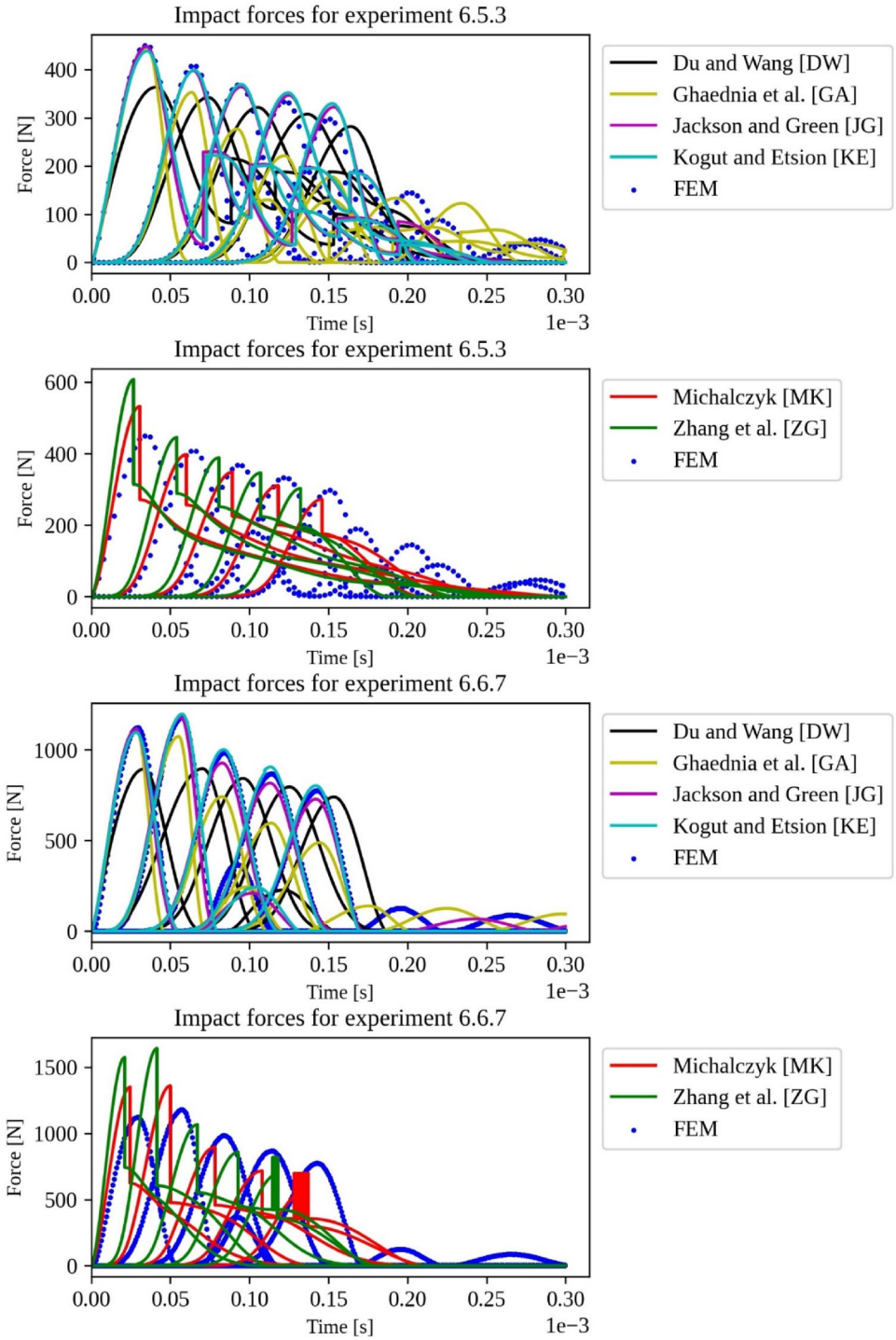

Fig. 15 Impact forces for numerical experiments in a 6 particle system part 4; for transparency the DW, GA, JG, KE MK and ZG models were separated

this was not investigated in this study. An exemplification of those effects can be observed in the impact force plots for experiments 6.4.7 and 6.5.3, which can be found in Figs. 14 and 15, respectively. In both cases, the initiating impact occurred between particles made of aluminium and steel, but in experiment 6.4.7 the other impacts involved only steel particles, whereas in experiment 6.5.3 subsequent impacts occurred only between aluminium particles. A comparative analysis of both plots shows significant differences in the evolution of impacts. In experiment 6.4.7 the higher inertia of the steel particles causes slower propagation of the impact wave. Because of this, the initiating impact ends before the second impact starts its restitution phase. As a result, although in this experiment the initiating velocity was higher than in experiment 6.5.3, all the impacts exhibit a scheme similar to

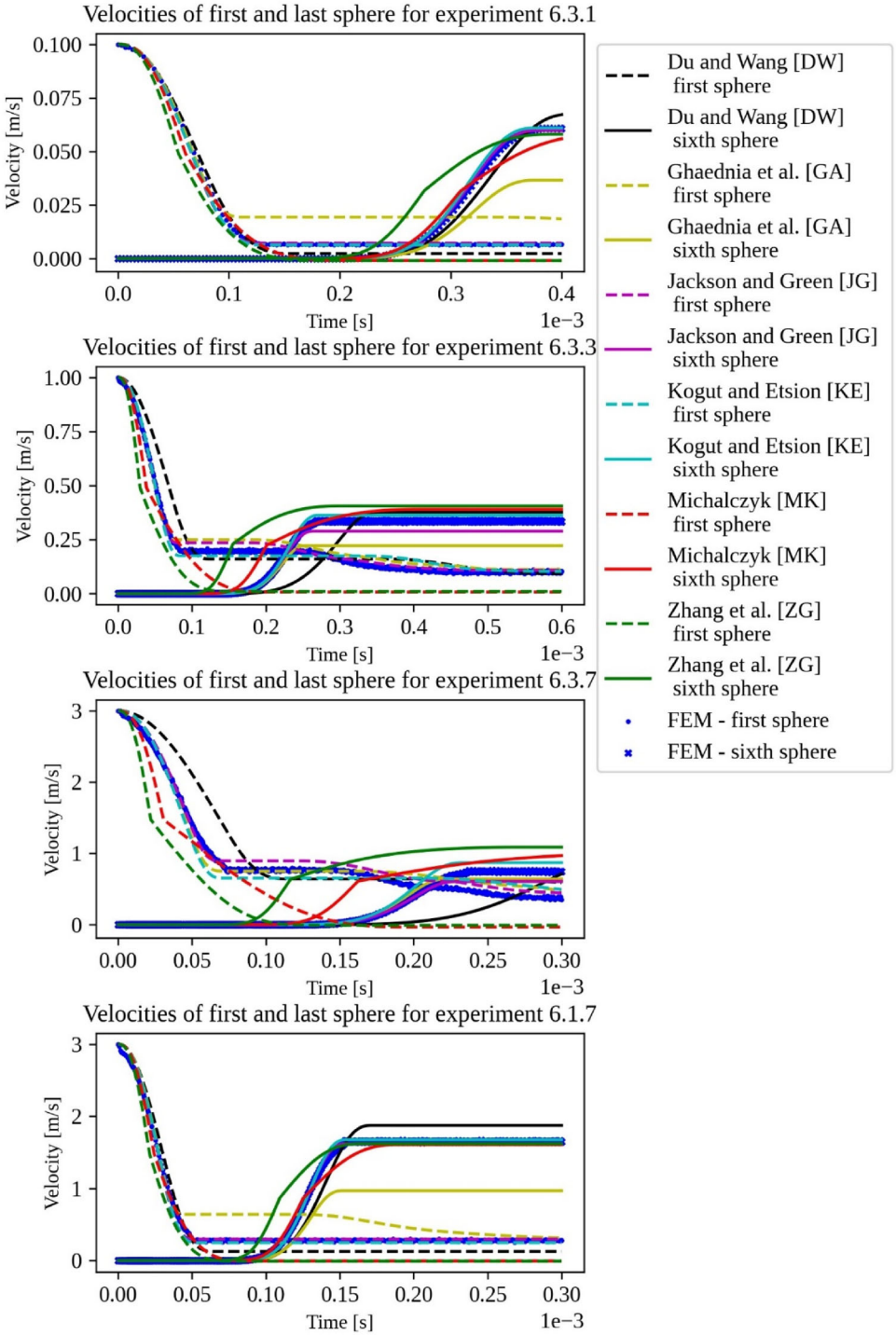

Fig. 16 Velocities for numerical experiments in a 6 particle system; data given for particles 1 and 6, part 1

simple, two-body impact, where there is only one compression and restitution phase. In contrast, in experiment 6.5.3 the aluminium particles are affected more rapidly by the initiating impact, which is why the second impact switches to the restitution phase during the restitution phase of the initiating impact, causing it to switch to the compression phase. This repeats for the subsequent impacts, causing substantially more complex behaviour than in experiment 6.4.7. Multiple switches between the restitution and compression phases take place, which generates many impact force discontinuities visible in the plot.

One possible solution of the impact force discontinuity problem may include an additional model feature used to identify the state from which the compression phase starts. If

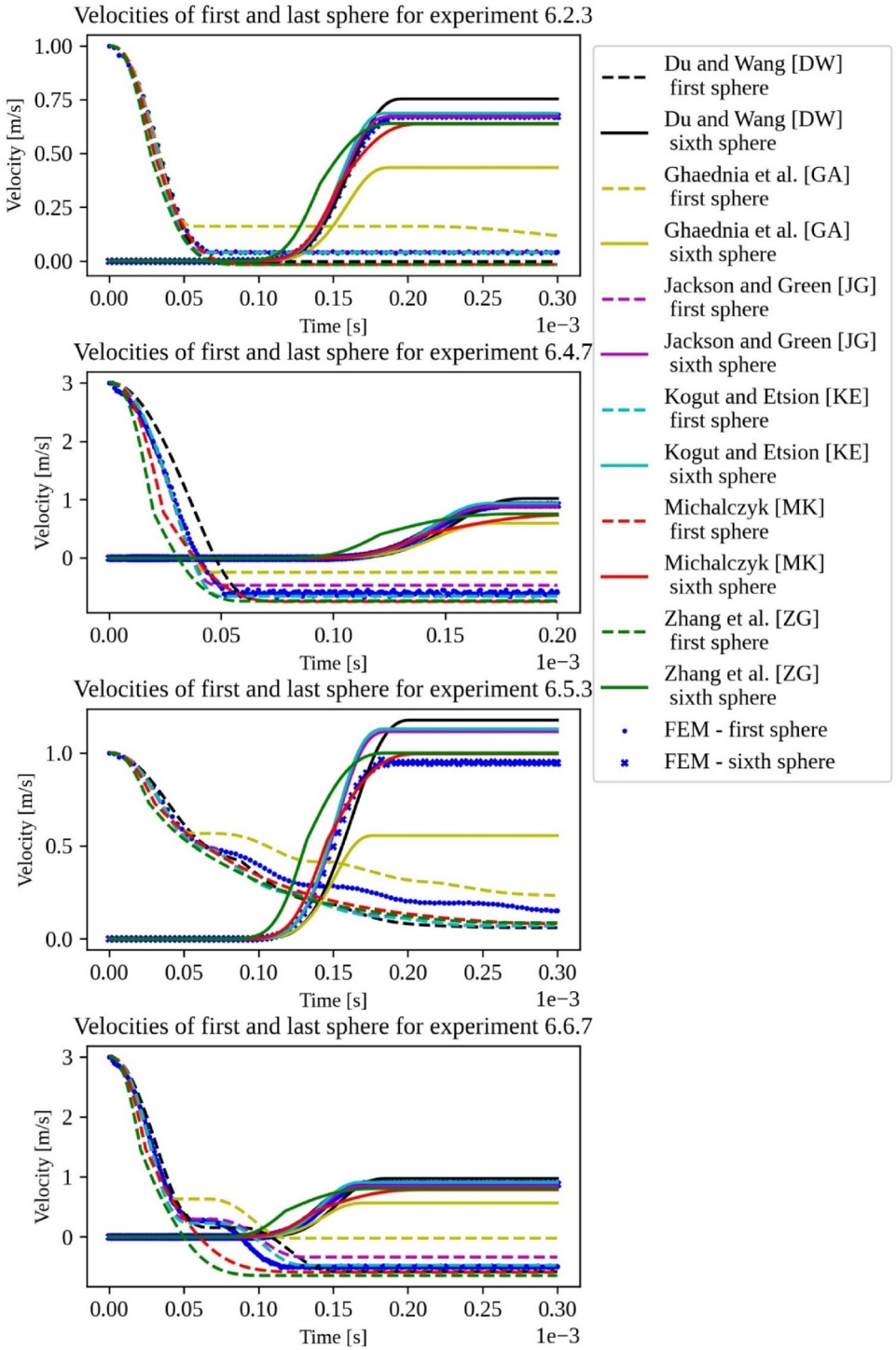

Fig. 17 Velocities for numerical experiments in a 6 particle system; data given for particles 1 and 6, part 2

the compression phase starts from the state at which no contact between the colliding bodies was detected, the contact force model should use its standard relation(s) for the compression phase. On the other hand, if the compression phase starts before the restitution phase has come to an end, the contact force model should use another mathematical relation to describe the force. It seems logical that this relation should be either the same as the one used for the restitution phase but limited to the maximal local deformation, which occurred during the previous compression phase, and followed in reverse direction, or ensures that for a given value of deformation the resulting force will be continuous. Although it seems a promising direction, further work is needed to confirm if it is worthwhile. Additionally, such an extension

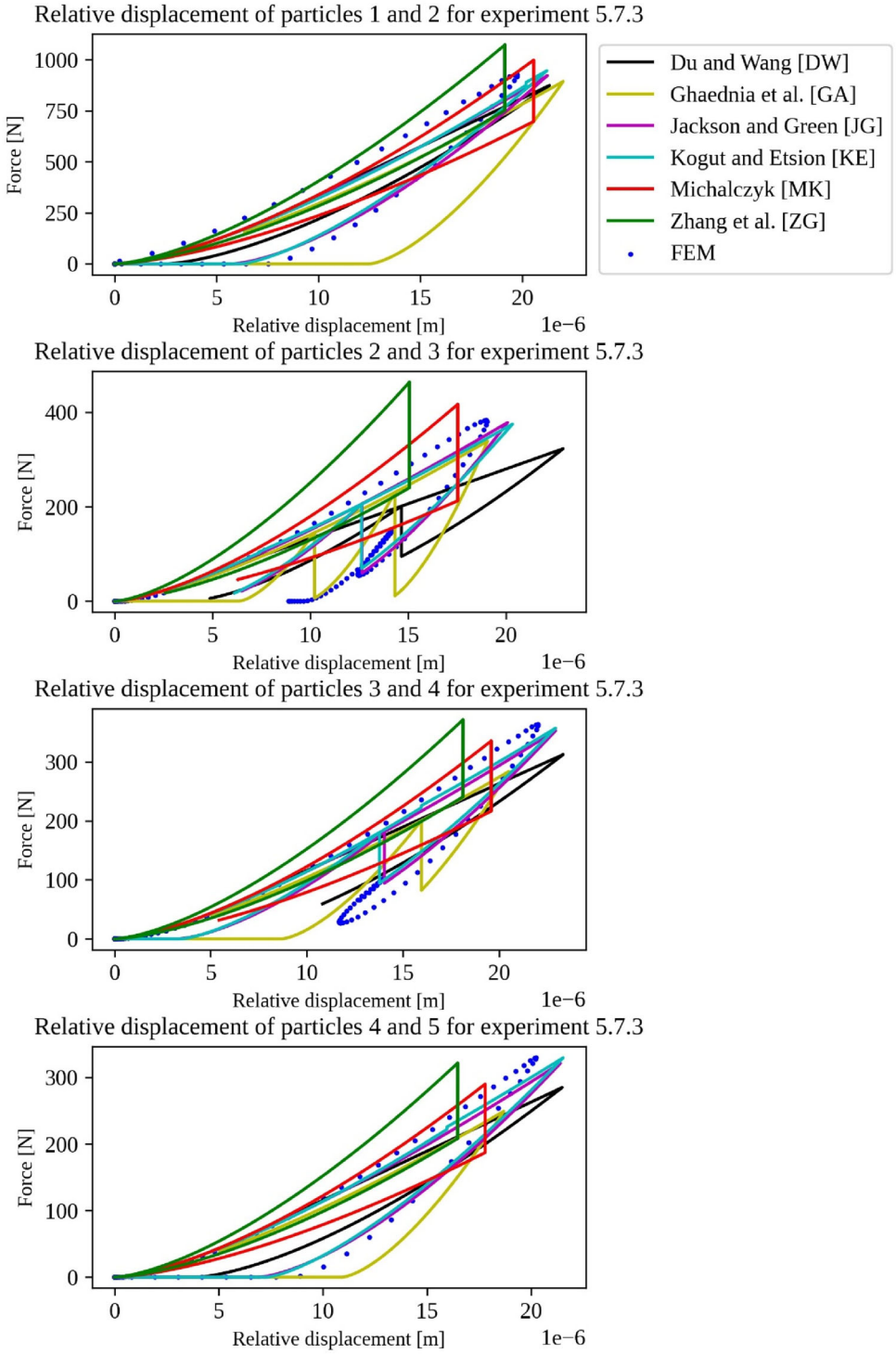

Fig. 18 Force–displacement relations for all impacts occurring during experiment 5.7.3

can cause challenges during software implementation of the improved models, as there will be a need to store and analyse previous system states. This will require another approach and algorithms for the solution of the differential equations describing the system. The mentioned challenges seem to be an interesting research opportunity and will be addressed by future works.

6 Conclusions

The contact force model plays a central role in impact modelling and is especially crucial in more complex cases of simultaneous, multi-zone collisions. The importance of this problem has been addressed by many researchers, who proposed various contact models, both new ones and some

offering incremental improvement. Those models, from a broad perspective, can be divided into two main groups when considering their approach to energy dissipation occurring during impact: using damping or plastic deformation. The present work analysed the contact force models belonging to both groups. In the preselection process, for which already published model comparisons were used, best candidates were selected. At this stage many Hunt and Crosley based models were excluded, as they require a priori knowledge about the initial impact velocity, which in the investigated cases was known only for the initiating impact. Because two of the preselected models (MK and ZG) required pre-restitution coefficients, they were calculated using a prepared FEM simulation. Furthermore, to check the correctness of each model implementation, numerical experiments for two-particle systems were carried out. It also allowed comparison of the COR values calculated by FEM simulation and those obtained by the investigated models (in the MK and ZG models, those were post- restitution coefficients). In the main part of this article, the ability to predict results of multi-zone, simultaneous impacts by the selected models were investigated using particle chains consisting of 3 to 6 particles made of three different materials: steel, aluminium, and bronze. To cover various levels of energy dissipation, three initial impact velocities were selected: 0.1 m/s, 1 m/s and 3 m/s.

The obtained results revealed substantial levels of error for all models, although some of them performed better than others. Considering the lowest average error of the predicted BVI, the KE and JG models achieved the best results with errors equal 3.89% and 4.15%, respectively. Nevertheless, the error increased with the growing number of particles and the increasing level of plasticity. The same models in their worst cases (numerical experiment 6.5.7) reached the error value of 38.66% and 33.77%, respectively. Such differences (or, in other words, high error variance) imply that care should be taken during the modelling of systems analogous to those investigated in this study and potential high levels of errors should be considered. The presented findings also suggest the necessity for improvement of the contact force models available in the literature.

Most of the published research uses simple systems consisting of two particles or a particle and a flat part for development and validation of the contact force model. This study is significantly different from those approaches, as it used a higher quantity of particles. It provided insight into the performance and behaviour of the selected contact force models in more complex systems. Considering the outcomes, it may be beneficial to include such cases in validation of the contact models proposed in future.

Further investigations are needed for better understanding of the phenomena occurring in multi-zone, simultaneous impacts and systems exhibiting such behaviour offer a promising direction in further research. Such systems also offer the opportunity for further improvement and refinement of existing contact force models or proposals of new ones. Those improvements may include better handling of the reversal to the compression phase during restitution, which may occur several times, an approach allowing calculation of the damping factor without a priori knowledge of the initial impact velocity, and replacement of constant COR with a function expressing it in the dependence on the impact velocity. The proposed changes will also require the development of new algorithms, as they may be more difficult to implement in software.

Funding This work was supported by the AGH University of Science and Technology with-in the scope of the research program No. 16.16.130.942.

Declarations

Conflict of interest The author has no competing interests to declare that are relevant to the content of this article.

References

1. Wan Q, Liu G, Song C, Zhou Y, Ma S, Tong R (2020) Study on the dynamic interaction of multiple clearance joints for flap actuation system with a modified contact force model. J Mech Sci Technol 34(7):2701–2713. https://doi.org/10.1007/s12206-020-0603-8
2. Guo K, Jiang N, Qi H, Feng Z, Wang Y, Tan W (2020) Experimental investigation of impact-sliding interaction and fretting wear between tubes and anti-vibration bars in steam generators. Nucl Eng Technol 52(6):1304–1317. https://doi.org/10.1016/j.net.2019.11.014
3. Zheng X, Li J, Wang Q, Liao Q (2019) A methodology for modeling and simulating frictional translational clearance joint in multibody systems including a flexible slider part. Mech Mach Theory 142:103603. https://doi.org/10.1016/j.mechmachtheory.2019.103603
4. Warzecha M, Michalczyk J (2020) Calculation of maximal collision force in kinematic chains based on collision force impulse. J Theor Appl Mech 58(2):339–349. https://doi.org/10.15632/jtam-pl/116580
5. Gharib M, Celik A, Hurmuzlu Y (2011) Shock absorption using linear particle chains with multiple impacts. J Appl Mech 78:031005. https://doi.org/10.1115/1.4003349

6. Gharib M, Karkoub M (2015) Shock-based experimental investigation of the linear particle chain impact damper. J Vib Acoust 137(6):061012. https://doi.org/10.1115/1.4031406
7. Meyer N, Seifried R (2021) Toward a design methodology for particle dampers by analyzing their energy dissipation. Comp Part Mech 8(4):681–699. https://doi.org/10.1007/s40571-020-00363-0
8. Burgoyne HA, Daraio C (2015) Elastic–plastic wave propagation in uniform and periodic granular chains. J Appl Mech 82(8):081002. https://doi.org/10.1115/1.4030458
9. Pal RK, Awasthi AP, Geubelle PH (2014) Characterization of wave propagation in elastic and elastoplastic granular chains. Phys Rev E 89(1):012204. https://doi.org/10.1103/PhysRevE.89.012204
10. Job S, Melo F, Sokolow A, Sen S (2007) Solitary wave trains in granular chains: experiments, theory and simulations. Granular Matter 10(1):13–20. https://doi.org/10.1007/s10035-007-0054-2
11. Daraio C, Nesterenko VF (2006) Strongly nonlinear wave dynamics in a chain of polymer coated beads. Phys Rev E 73(2):026612. https://doi.org/10.1103/PhysRevE.73.026612
12. Daraio C, Nesterenko VF, Herbold EB, Jin S (2006) Energy trapping and shock disintegration in a composite granular medium. Phys Rev Lett 96(5):058002. https://doi.org/10.1103/PhysRevLett.96.058002
13. Cante J et al (2014) PFEM-based modeling of industrial granular flows. Comp Part Mech 1(1):47–70. https://doi.org/10.1007/s40571-014-0004-9
14. Izard E, Hamouda HB, Voorde JV (2021) High-stress impact–abrasion test by discrete element modeling. Comp Part Mech 8(5):1061–1073. https://doi.org/10.1007/s40571-020-00377-8
15. Yu R, Dong X, Li Z, Fan M (2023) A coupled SPH–DEM model for erosion process of solid surface by abrasive water-jet impact. Comp Part Mech. https://doi.org/10.1007/s40571-023-00555-4
16. Berry N, Zhang Y, Haeri S (2023) Contact models for the multi-sphere discrete element method. Powder Technol 416:118209. https://doi.org/10.1016/j.powtec.2022.118209
17. Kildashti K, Dong K, Yu A (2023) Contact force models for non-spherical particles with different surface properties: a review. Powder Technol 418:118323. https://doi.org/10.1016/j.powtec.2023.118323
18. Deskiewicz A, Perz R (2017) Agricultural aircraft wing slat tolerance for bird strike. AEAT 89(4):590–598. https://doi.org/10.1108/AEAT-11-2016-0220
19. Jastrzębski D, Perz R (2020) Rib kinematics analysis in oblique and lateral impact tests. Acta Bioeng Biomech. https://doi.org/10.37190/ABB-01431-2019-03
20. Sun Y, Shi F, Zhang S, Wang H, Xing M (2023) Improving the robustness of non-Hertzian wheel–rail contact model for railway vehicle dynamics simulation. Multibody Syst Dyn. https://doi.org/10.1007/s11044-023-09903-x
21. Baeza L, Bruni S, Giner-Navarro J, Liu B (2023) A linear non-Hertzian unsteady tangential wheel-rail contact model. Tribol Int 181:108345. https://doi.org/10.1016/j.triboint.2023.108345
22. Han I, Gilmore BJ (1993) Multi-body impact motion with friction—analysis, simulation, and experimental validation. J Mech Des 115(3):412–422
23. Pereira MS, Nikravesh P (1996) Impact dynamics of multibody systems with frictional contact using joint coordinates and canonical equations of motion. Nonlinear Dyn 9(1–2):53–71
24. Glocker Ch, Pfeiffer F (1995) Multiple impacts with friction in rigid multibody systems. Nonlinear Dyn 7(4):471–497
25. Adams GG (1997) Imperfectly constrained planer impacts: a coefficient-of-restitution model. Int J Impact Eng 19(8):693–701
26. Stronge WJ (2000) Chain reaction from impact on coaxial multibody systems. J Appl Mech 67(3):632–635. https://doi.org/10.1115/1.1309541
27. Stronge WJ (2018) Impact mechanics. Cambridge University Press, Cambridge
28. Hertz H (1882) Ueber die Berührung fester elastischer Körper. J für die reine Angew Math (Crelles J) 1882(92):156–171. https://doi.org/10.1515/crll.1882.92.156
29. Hunt KH, Crossley FRE (1975) Coefficient of restitution interpreted as damping in vibroimpact. J Appl Mech 42(2):440–445. https://doi.org/10.1115/1.3423596
30. Flores P, Machado M, Silva MT, Martins JM (2011) On the continuous contact force models for soft materials in multibody dynamics. Multibody Syst Dyn 25(3):357–375. https://doi.org/10.1007/s11044-010-9237-4
31. Hu S, Guo X (2015) A dissipative contact force model for impact analysis in multibody dynamics. Multibody Syst Dyn 35(2):131–151. https://doi.org/10.1007/s11044-015-9453-z
32. Carvalho AS, Martins JM (2019) Exact restitution and generalizations for the Hunt-Crossley contact model. Mech Mach Theory 139:174–194. https://doi.org/10.1016/j.mechmachtheory.2019.03.028
33. Kogut L, Etsion I (2002) Elastic-plastic contact analysis of a sphere and a rigid flat. J Appl Mech 69(5):657–662. https://doi.org/10.1115/1.1490373
34. Ghaednia H, Brake MRW, Berryhill M, Jackson RL (2019) Strain hardening from elastic–perfectly plastic to perfectly elastic flattening single asperity contact. J Tribol 141(3):031402. https://doi.org/10.1115/1.4041537
35. Jackson RL, Green I (2005) A finite element study of elasto-plastic hemispherical contact against a rigid flat. J Tribol 127(2):343–354. https://doi.org/10.1115/1.1866166
36. Gilardi G, Sharf I (2002) Literature survey of contact dynamics modelling. Mech Mach Theory 37(10):1213–1239. https://doi.org/10.1016/S0094-114X(02)00045-9
37. Machado M, Moreira P, Flores P, Lankarani HM (2012) Compliant contact force models in multibody dynamics: evolution of the Hertz contact theory. Mech Mach Theory 53:99–121
38. Khulief YA (2013) Modeling of impact in multibody systems: an overview. J Comput Nonlinear Dyn 8:021012
39. Thornton C, Cummins SJ, Cleary PW (2013) An investigation of the comparative behaviour of alternative contact force models during inelastic collisions. Powder Technol 233:30–46
40. Alves J, Peixinho N, da Silva MT, Flores P, Lankarani HM (2015) A comparative study of the viscoelastic constitutive models for frictionless contact interfaces in solids. Mech Mach Theory 85:172–188. https://doi.org/10.1016/j.mechmachtheory.2014.11.020
41. Banerjee A, Chanda A, Das R (2017) Historical origin and eecent development on normal directional impact models for rigid body contact simulation: a critical review. Arch Comput Methods Eng 24(2):397–422. https://doi.org/10.1007/s11831-016-9164-5
42. Jankowski R (2005) Non-linear viscoelastic modelling of earthquake-induced structural pounding. Earthq Eng Struct Dyn 34(6):595–611. https://doi.org/10.1002/eqe.434
43. Ghaednia H, Wang X, Saha S, Xu Y, Sharma A, Jackson RL (2017) A review of elastic–plastic contact mechanics. Appl Mech Rev 69(6):060804. https://doi.org/10.1115/1.4038187
44. Skrinjar L, Slavič J, Boltežar M (2018) A review of continuous contact-force models in multibody dynamics. Int J Mech Sci 145:171–187. https://doi.org/10.1016/j.ijmecsci.2018.07.010
45. Xiang D, Shen Y, Wei Y, You M (2018) A comparative study of the dissipative contact force models for collision under external spring forces. J Comput Nonlinear Dyn. https://doi.org/10.1115/1.4041031
46. Jian B, Hu GM, Fang ZQ, Zhou HJ, Xia R (2019) Comparative behavior of damping terms of viscoelastic contact force models with consideration on relaxation time. Powder Technol 356:735–749. https://doi.org/10.1016/j.powtec.2019.08.110
47. Ding S, Jian B, Zhang Y, Xia R, Hu G (2023) A normal contact force model for viscoelastic bodies and its finite element modeling

verification. Mech Mach Theory 181:105202. https://doi.org/10.1016/j.mechmachtheory.2022.105202
48. Zhang J, Fang M, Zhao L, Zhao Q, Liang X, He G (2022) A continuous contact force model for the impact analysis of hard and soft materials. Mech Mach Theory 177:105065. https://doi.org/10.1016/j.mechmachtheory.2022.105065
49. Stronge WJ (1999) Mechanics of impact for compliant multi-body systems. In: Pfeiffer F and Glocker C, (eds) IUTAM symposium on unilateral multibody contacts, solid mechanics and its applications, vol. 72. Springer: Dordrecht, Netherlands, pp. 137–144
50. Carretero-González R, Khatri D, Porter MA, Kevrekidis PG, Daraio C (2009) Dissipative solitary waves in granular crystals. Phys Rev Lett 102(2):024102. https://doi.org/10.1103/PhysRevLett.102.024102
51. Burgoyne HA, Daraio C (2014) Strain-rate-dependent model for the dynamic compression of elastoplastic spheres. Phys Rev E 89(3):032203. https://doi.org/10.1103/PhysRevE.89.032203
52. Feng Y, Kang W, Ma D, Liu C (2019) Multiple impacts and multiple-compression process in the dynamics of granular chains. J Comput Nonlinear Dyn 14(12):121002. https://doi.org/10.1115/1.4044584
53. Herbert RG, McWhannell DC (1977) Shape and frequency composition of pulses from an impact pair. J Eng Ind 99(3):513–518. https://doi.org/10.1115/1.3439270
54. Lee TW, Wang AC (1983) On the dynamics of intermittent-motion mechanisms. Part 1: dynamic model and response. J Mech Transm Autom Des 105(3):534–540. https://doi.org/10.1115/1.3267392
55. Lankarani HM, Nikravesh PE (1990) A contact force model with hysteresis damping for impact analysis of multibody systems. J Mech Des 112(3):369–376. https://doi.org/10.1115/1.2912617
56. Gonthier Y, McPhee J, Lange C, Piedbœuf J-C (2004) A regularized contact model with asymmetric damping and dwell-time dependent friction. Multibody SysDyn 11(3):209–233. https://doi.org/10.1023/B:MUBO.0000029392.21648.bc
57. Zhiying Q, Qishao L (2006) Analysis of impact process based on restitution coefficient. J Dyn Control 4:294–298
58. Shen Y, Xiang D, Wang X, Jiang L, Wei Y (2018) A contact force model considering constant external forces for impact analysis in multibody dynamics. Multibody Syst Dyn 44(4):397–419. https://doi.org/10.1007/s11044-018-09638-0
59. Safaeifar H, Farshidianfar A (2020) A new model of the contact force for the collision between two solid bodies. Multibody Syst Dyn. https://doi.org/10.1007/s11044-020-09732-2
60. Zhang J, Li W, Zhao L, He G (2020) A continuous contact force model for impact analysis in multibody dynamics. Mech Mach Theory 153:103946. https://doi.org/10.1016/j.mechmachtheory.2020.103946
61. da Silva MR, Marques F, da Silva MT, Flores P (2022) A compendium of contact force models inspired by Hunt and Crossley's cornerstone work. Mech Mach Theory 167:104501. https://doi.org/10.1016/j.mechmachtheory.2021.104501
62. Flores P, Ambrósio J, Lankarani HM (2023) Contact-impact events with friction in multibody dynamics: back to basics. Mech Mach Theory 184:105305. https://doi.org/10.1016/j.mechmachtheory.2023.105305
63. Michalczyk J (2008) Phenomenon of force impulse restitution in collision modelling. J Theor Appl Mech 46(4):897–908
64. Zhang X, Vu-Quoc L (2002) Modeling the dependence of the coefficient of restitution on the impact velocity in elasto-plastic collisions. Int J Impact Eng 27(3):317–341. https://doi.org/10.1016/S0734-743X(01)00052-5
65. Etsion I, Kligerman Y, Kadin Y (2005) Unloading of an elastic–plastic loaded spherical contact. Int J Solids Struct 42(13):3716–3729. https://doi.org/10.1016/j.ijsolstr.2004.12.006
66. Du Y, Wang S (2009) Energy dissipation in normal elastoplastic impact between two spheres. J Appl Mech 76(6):061010
67. Jackson RL, Green I, Marghitu DB (2010) Predicting the coefficient of restitution of impacting elastic-perfectly plastic spheres. Nonlinear Dyn 60(3):217–229. https://doi.org/10.1007/s11071-009-9591-z
68. Ghaednia H, Marghitu DB, Jackson RL (2014) Predicting the permanent deformation after the impact of a rod with a flat surface. J Tribol 137:011403. https://doi.org/10.1115/1.4028709
69. Ghaednia H, Pope SA, Jackson RL, Marghitu DB (2016) A comprehensive study of the elasto-plastic contact of a sphere and a flat. Tribol Int 93:78–90. https://doi.org/10.1016/j.triboint.2015.09.005
70. Brake MR (2012) An analytical elastic-perfectly plastic contact model. Int J Solids Struct 49(22):3129–3141. https://doi.org/10.1016/j.ijsolstr.2012.06.013
71. Brake MR (2015) An analytical elastic plastic contact model with strain hardening and frictional effects for normal and oblique impacts. Int J Solids Struct 62:104–123
72. Ghaednia H, Cermik O, Marghitu DB (2015) Experimental and theoretical study of the oblique impact of a tennis ball with a racket. Proc IMechE 229(3):149–158. https://doi.org/10.1177/1754337114567490
73. Jackson RL, Kogut L (2006) A comparison of flattening and indentation approaches for contact mechanics modeling of single asperity contacts. J Tribol 128(1):209–212. https://doi.org/10.1115/1.2114948
74. Wang H, Yin X, Hao H, Chen W, Yu B (2020) The correlation of theoretical contact models for normal elastic-plastic impacts. Int J Solids Struct 182–183:15–33. https://doi.org/10.1016/j.ijsolstr.2019.07.018
75. Minamoto H, Kawamura S (2009) Effects of material strain rate sensitivity in low speed impact between two identical spheres. Int J Impact Eng 36(5):680–686. https://doi.org/10.1016/j.ijimpeng.2008.10.001
76. Geuzaine C, Remacle J-F (2009) Gmsh: A 3-D finite element mesh generator with built-in pre- and post-processing facilities: the GMSH paper. Int J Numer Meth Engng 79(11):1309–1331. https://doi.org/10.1002/nme.2579
77. Electricité de France (1989) Finite element code_aster, analysis of structures and thermomechanics for studies and research